COGEU

FP7 ICT-2009.1.1

COgnitive radio systems for efficient sharing of TV white spaces in EUropean context

COGEU D5.4
COGEU TVWS Transceiver Performance Evaluation

Contractual Date of Delivery to the CEC: October 2012

Actual Date of Delivery to the CEC: October 2012

Author(s): Tim Forde (TCD), Justin Tallon (TCD), Linda Doyle (TCD), Pawel Kryszkiewicz (PUT), Hanna Bogucka (PUT), Adrian Kliks (PUT).

Participant(s): TCD, PUT

Workpackage: WP5

Est. person months: 13

Security: PU

Nature: Report

Version: 0.1

Total number of pages: 43

Abstract:

This deliverable reports on the work performed in COGEU task T5.5. It describes the investigation and perfromance evaluation of the spectrum shaping and Rendezvous components; yielding performance statistics for both components under a range of scenarios. Experimentation was undertaken in TV Band frequencies. The RF frontend of the USRP has been characterised and modified to allow for improved transmission at higher powers such that transmit-side signal distortion of OFDM-based waveforms was minimised.

Keyword list: TVWS, Transceiver, SDR, OFDM, USRP, GNU Radio, IRIS, Spectrum Shaping, Rendezvous.

Executive Summary

This deliverable addresses one task, the evaluation of the performance of the TVWS Transceiver, with particular attention paid to the spectrum shaping and rendezvous components of the system. The key conclusions of this deliverable are summarized here.

RF Frontend

The WBX RF daughterboard, used to transmit and receive in the TV Band frequencies, has been characterized and modified to allow for better performance at our experimental frequencies. The amplifier modifications allow for transmission of complex OFDM-based waveforms at higher power without distorting the transmitted signal.

Spectrum Shaping

The spectrum shaping mechanisms selected for use in the COGEU project have been shown to work efficiently under certain limitations caused by the USRP frontend (intermodulations, only some sampling frequencies allowed), and the host PC (computational complexity).

The link capacity has been shown to be only slightly dependent on spectrum shaping algorithms (throughput decrease because of CCs and windowing introduction, SNR loss negligible).

It has been shown that time domain synchronization can be disturbed by CCs (we can turn them off only in the preamble) and interference from primary systems. An efficient synchronization strategy under strong interference from primary devices is required. In the current system we have determined the requirement for a 20 dB SIR for correct transmission in the presence of PMSE device.

It has also been shown that spectrum shaping gives improvement not only in the PSD plot, but also for end-user QoS experience. With the same spectrum occupation (narrow notch) we can increase secondary user power by e.g. 8 dB providing the same sound quality to PMSE device user.

Rendezvous

The performance of the Rendezvous component has been evaluated in the TV Band at 706MHz. The component was evaluated with respect to its Time To Rendezvous performance, i.e. the time it takes a slave device to find a master device's embedded signature in a signal. It has also been evaluated with respect to the reliability and accuracy of the detector. The implication of a bursty signature presence was also evaluated to stress the robustness of the detector implementation.

The optimal range for the observation window setting was determined such that the TTR is minimized; experiments for a range of scenarios were undertaken and a radio designer can use these measurements to inform a radio control module to tune the Rendezvous component appropriately. The window range was also determined for a range of signature sizes. The instability brought about by signals containing the signature for a duty cycle of less than 80% was found; this instability can be corrected by allowing for a larger observation window.

The reliability and accuracy of the detector was also assessed and probability of detection and probability of false alarm graphs for a range of scenarios are presented. The experiments indicate that the when the detector decision is set appropriately that it is possible to achieve 100% reliability for an observation window setting that also ensures minimal TTR.

Table of Contents

1- Introduction

This deliverable relates to the performance evaluation of the TVWS Transceiver carried out as part of T5.5. Performance evaluation work has already been described in D5.2 (Algorithms for cognitive spectrum shaping and advanced rendezvous) [1] and D5.3 (COGEU TVWS transceiver integration) [2]; such evaluation was necessary as the TVWS Transceiver was being developed. This deliverable extends that reported work using the mature TVWS prototype transceiver.

The TVWS Transceiver is designed to address a specific application and to provide a platform to demonstrate some key aspects of a TV whitespace device that enable it to both safely and efficiently use TVWS opportunities. The TVWS prototype uses the experimental software radio-based system described in Deliverable 5.1 [3]; principally the Iris software radio and the USRP RF frontend.

The transceiver has multiple objectives; a number of distinct components have been developed to address these objectives. Principally, spectrum shaping and rendezvous components have been developed and are addressed in this deliverable. While these components operate together to effect the safe and dynamic use of spectrum, they are evaluated separately as they are independent components whose operation is not co-dependent.

Additionally, some modifications have been made to the WBX RF frontend. Our experience of using the WBX in field experiments led us to investigate its operation more closely. In Chapter 2 we describe some modifications that we have made to TVWS Transceiver to improve our use of it in the TV Bands.

In Chapter 3 the results of the Spectrum Shaping component evaluation are presented. The spectrum shaping implementation is evaluated with regard to its ability to efficiently comply with Block Edge Mask constraints which would be set by regulators. The link capacity of shaped OFDM transmissions is also investigated. Finally, the impact of TVWS Transceiver transmissions on PMSE devices is evaluated.

Finally, in Chapter 4 the performance of the Rendezvous component implementation is investigated in the TV Band. The key performance metrics for this component, the TTR and the detector reliability, are evaluated at 706MHz for a range of scenarios in which key parameters of the detector are tuned to different settings. The performance envelope for these scenarios is presented and the optimum range of the tunable parameters for the operation for the detector is indicated.

2- RF Frontend WBX Characterisation, Modification for TVWS use

As described in Deliverable 5.1 [3], the COGEU TVWS device is a software radio which is enabled by combining Iris with an Ettus LLC Universal Software Radio Peripheral (USRP). In order to access the TV bands a WBX RF daughterboard is employed.

Over the course of our development of the Iris-based components we observed the characteristics of the TVWS device. As we encountered difficulties in increasing the power of the TVWS Transceiver during the Munich trials, reported on in WP7, we investigated an alternative approach to increasing the output power up to the limit of our licence.

While the WBX has an operational transmit range from 50MHz to 2.2GHz, when it came to evaluating our components in the TV band towards the end of the project, we obtained a licence from the Irish spectrum regulator to operate between 694 MHz and 718MHz with a maximum transmission power of 100mW.

2.1- Increasing output power

In the course of experimenting with the WBX boards we found that amplification of the signal using the in-built WBX amplifier sometimes resulted in distortion of the OFDM-based waveforms such that the these signals could not be demodulated by the receivers at low receive powers. In particular, our experience of the higher-power trials in Munich alerted us to issues with transmitter signal distortion and consequent issues for receiver sensitivity when the on-board WBX gain was set too high for certain OFDM-based wave-forms.

So, in order to increase the output power of the USRP to 20dBm (100mW) for the TV bands, in particular the 694-718 MHz, we choose to use an external amplifier. Currently, we limit the output power to ~2dBm for an OFDM signal on a WBX daughterboard at which level there is no distortion. Increasing the output power by 20dB would theoretically result in a tenfold increase in free space range.

The simplest way to increase output power is by placing a suitable COTS amplifier in line with the USRP/WBX transmit output. Since it's necessary to amplify complex signals with high peak to average power ratios, the amplifier should allow for about 6dB back-off from maximum power at 20dBm output, that is, the amplifier should be rated at 26dBm for 694-718MHz. The gain also needs to be greater than 20dB. Fine output power adjustment can be done on the USRP.

The ZFL-2500VH+ from Mini-circuits (www.minicircuits.com) meets the above requirement based on typical performance; see the amplifier characteristics specified in Figure 2-1. It also has the advantage that it covers frequencies up to 2500MHz, which makes it suitable for use in the WiFi – 802.11 band should experimentation in those bands be necessary. The amplifier requires a separate +15V DC power supply.

FREQUENCY (MHz)	GAIN (dB)			DIRECTIVITY (dB)			VSWR (:1)		NOISE FIGURE (dB)	POUT at 1 dB COMPR. (dBm)
	12V	15V	16V	12V	15V	16V	IN	OUT	15V	15V
10.00	24.67	24.50	24.32	17.40	18.30	18.60	1.25	1.56	6.31	26.96
173.30	24.75	25.24	25.12	17.10	16.70	16.50	1.27	1.32	4.86	27.17
336.70	24.83	25.31	25.18	16.80	15.70	16.10	1.32	1.30	4.99	27.13
500.00	24.95	25.45	25.34	15.40	14.80	15.00	1.37	1.25	5.00	27.07
510.00	24.97	25.45	25.32	16.10	16.30	15.40	1.38	1.24	5.00	27.09
673.30	24.80	25.70	25.62	16.30	13.80	13.70	1.40	1.17	5.00	26.91
836.70	24.90	25.34	25.22	16.00	13.40	14.20	1.38	1.09	4.95	26.51
1000.00	25.00	25.42	25.35	15.40	13.30	13.30	1.37	1.08	4.93	26.30
1010.00	25.13	25.46	25.38	15.80	13.70	13.10	1.37	1.08	4.97	26.31
1173.30	25.04	25.84	25.74	15.60	13.70	14.00	1.40	1.10	4.98	26.25
1336.70	25.29	25.79	25.69	15.70	14.40	14.30	1.36	1.10	5.01	26.11
1500.00	25.00	25.58	25.47	16.00	15.30	14.80	1.27	1.11	5.08	25.78
1510.00	24.98	25.57	25.47	15.90	15.40	15.80	1.26	1.11	5.10	25.79
1673.30	25.16	25.53	25.40	15.60	15.20	15.20	1.16	1.15	5.12	25.25
1836.70	24.85	25.36	25.26	15.70	15.70	15.10	1.16	1.20	5.13	24.66
2000.00	24.81	25.35	25.21	14.90	15.80	16.80	1.19	1.25	5.11	25.48
2010.00	24.76	25.28	25.15	15.40	16.40	16.20	1.19	1.26	5.13	25.53
2173.30	24.46	25.57	25.44	15.40	15.60	15.90	1.20	1.33	5.16	26.08
2336.70	24.32	25.41	25.25	15.40	16.50	17.30	1.22	1.46	5.26	26.09
2500.00	23.94	25.62	25.42	15.20	16.60	17.90	1.26	1.71	5.18	25.81

Figure 2-1 ZFL-2500VH+ amplification characteristics

2.2- **Spurious signals: WBX Harmonics, local oscillator**

In the course of investigating the use of the WBX RF daughter board at higher output powers we had to consider spurious emissions. There are 2 main types of spurious to consider; in-band and out-of-band. In the case of the work that took place in Ireland, the frequency range 694-718 MHz can be considered in-band and anything outside this band is obviously out-of-band spurious.

On investigation of the WBX frontend it was found that there are a number of signals that should be considered and dealt with appropriately. Plots of the wanted signal (Figure 2-2), and in-band (Figure 2-3) and out-of-band (Figure 2-4) spurious signals are shown. For the in-band case it is necessary to choose the “offset” to keep the LO spurious and the image inside the band. It is not possible to filter these out with a *simple* RF filter.

For the out-of-band case, there are quite large spurious at multiples of the output frequency (not strictly harmonics); these can be seen clearly in the third plot, Figure 2-4. Most worrying of these is a -16dBm spur at 2138MHz (UMTS/IMT/3G band), shown in Figure 2-5. This would also be amplified by at least 20dB by the new PA. As it stands these spurs are already too high for a demonstration and were required to be filtered. Note that in the Munich trials a cavity filter was employed to guard against out-of-band WBX emissions.

A band pass filter was chosen to remove any low frequency spurious from digital circuits, crystal oscillators etc. As a suitable COTS band pass filter couldn’t be found, one was designed and built specifically for the frequencies licensed to us for demonstration.

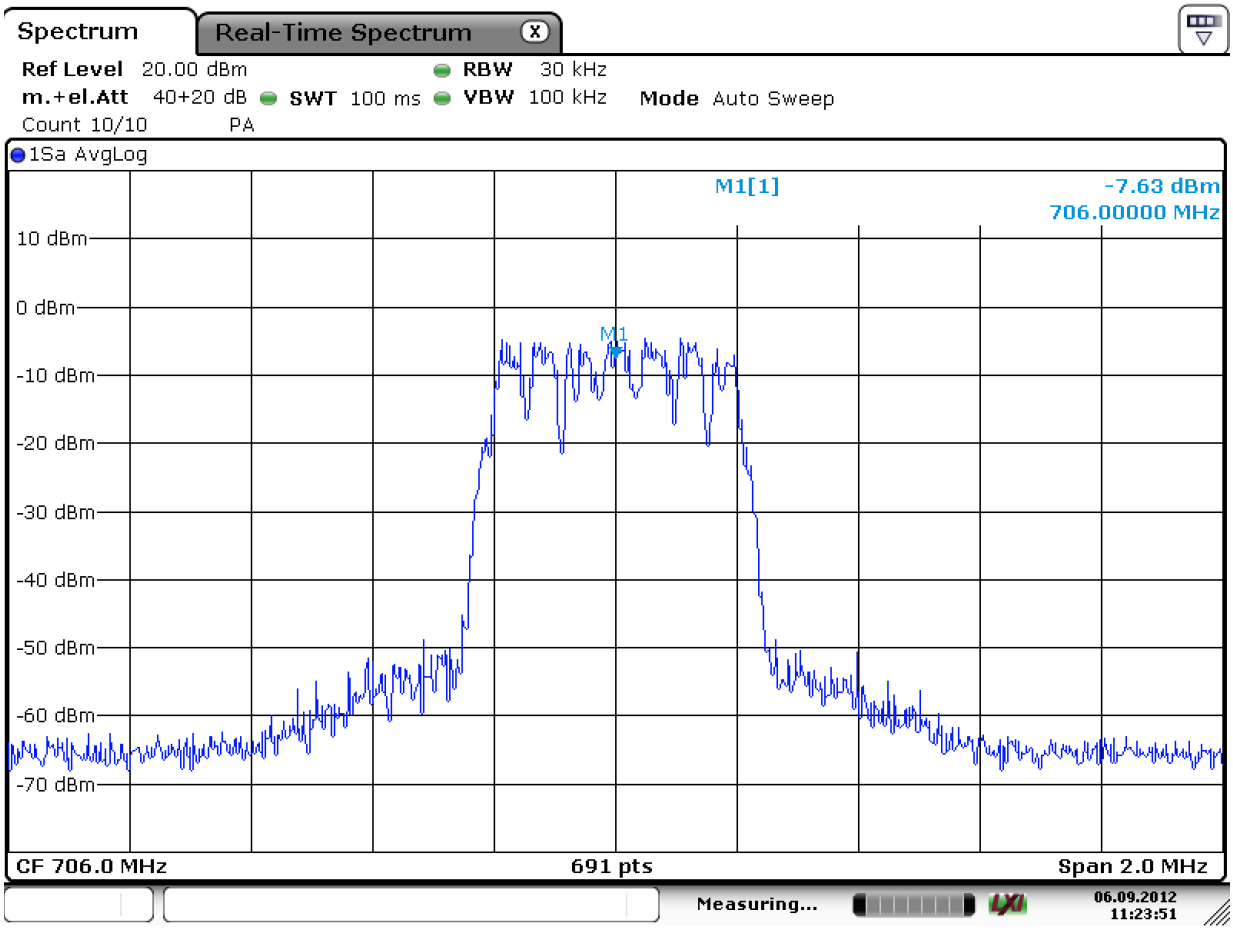

Figure 2-2 Wanted signal

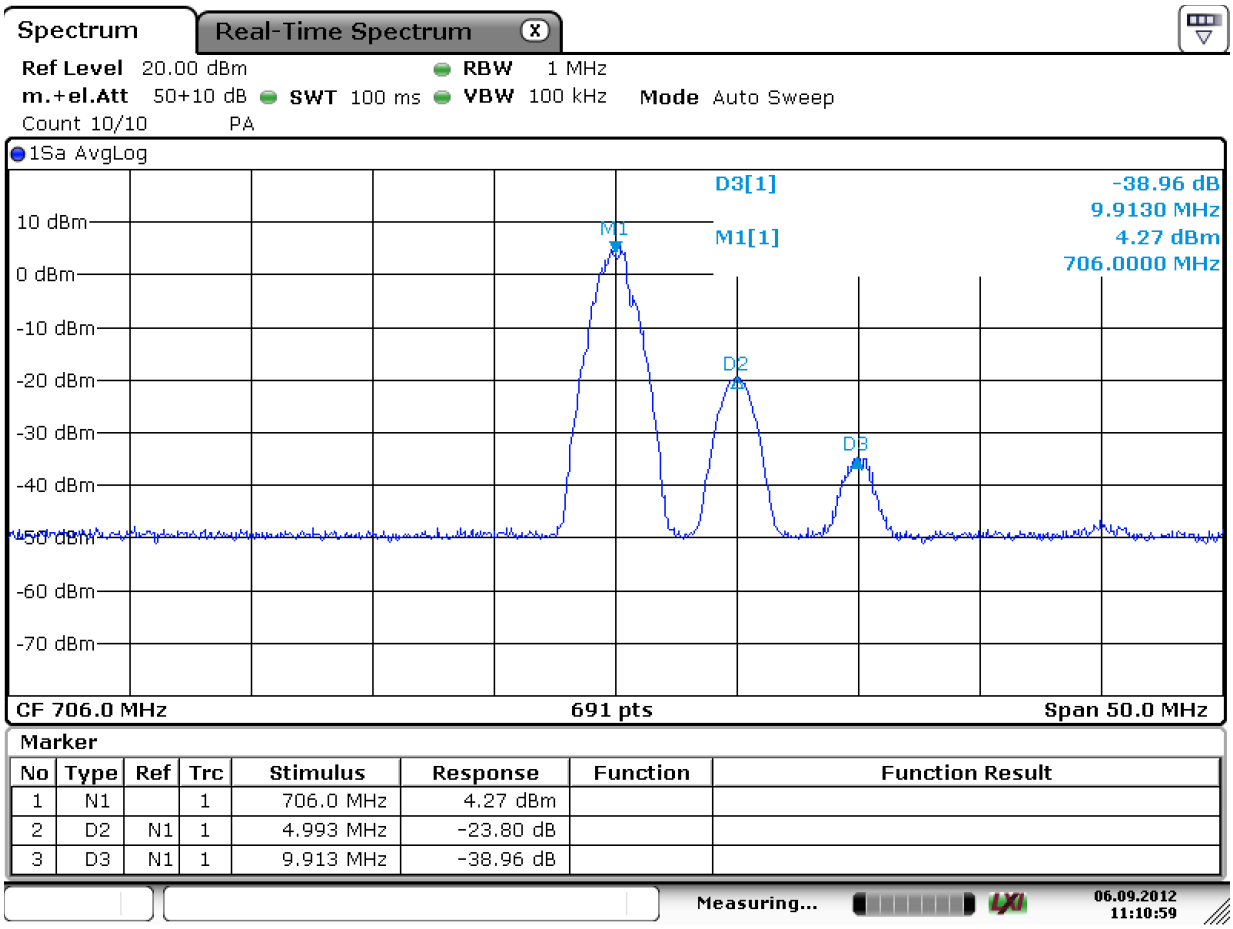

Figure 2-3 Unwanted in-band signals

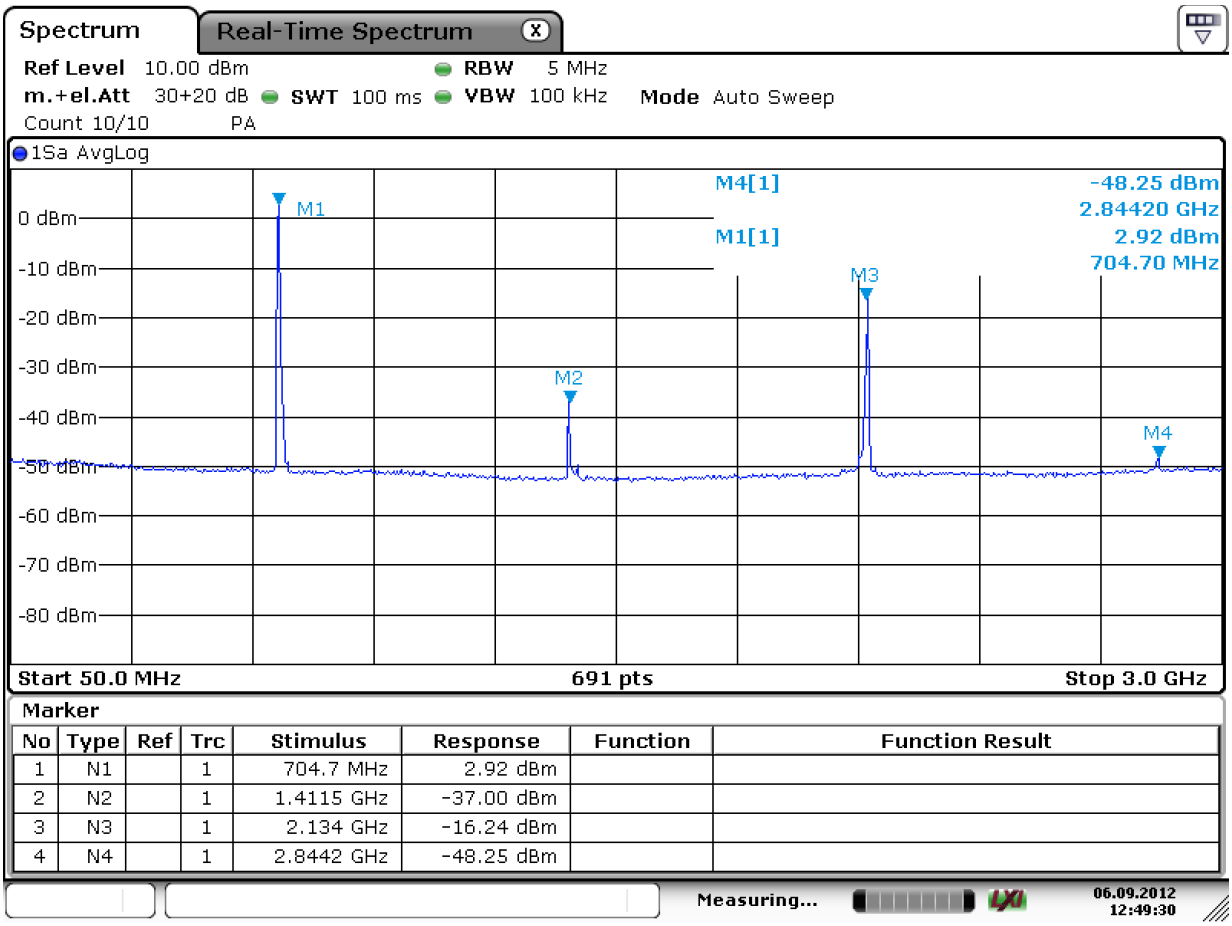

Figure 2-4 Unwanted out-of-band signals

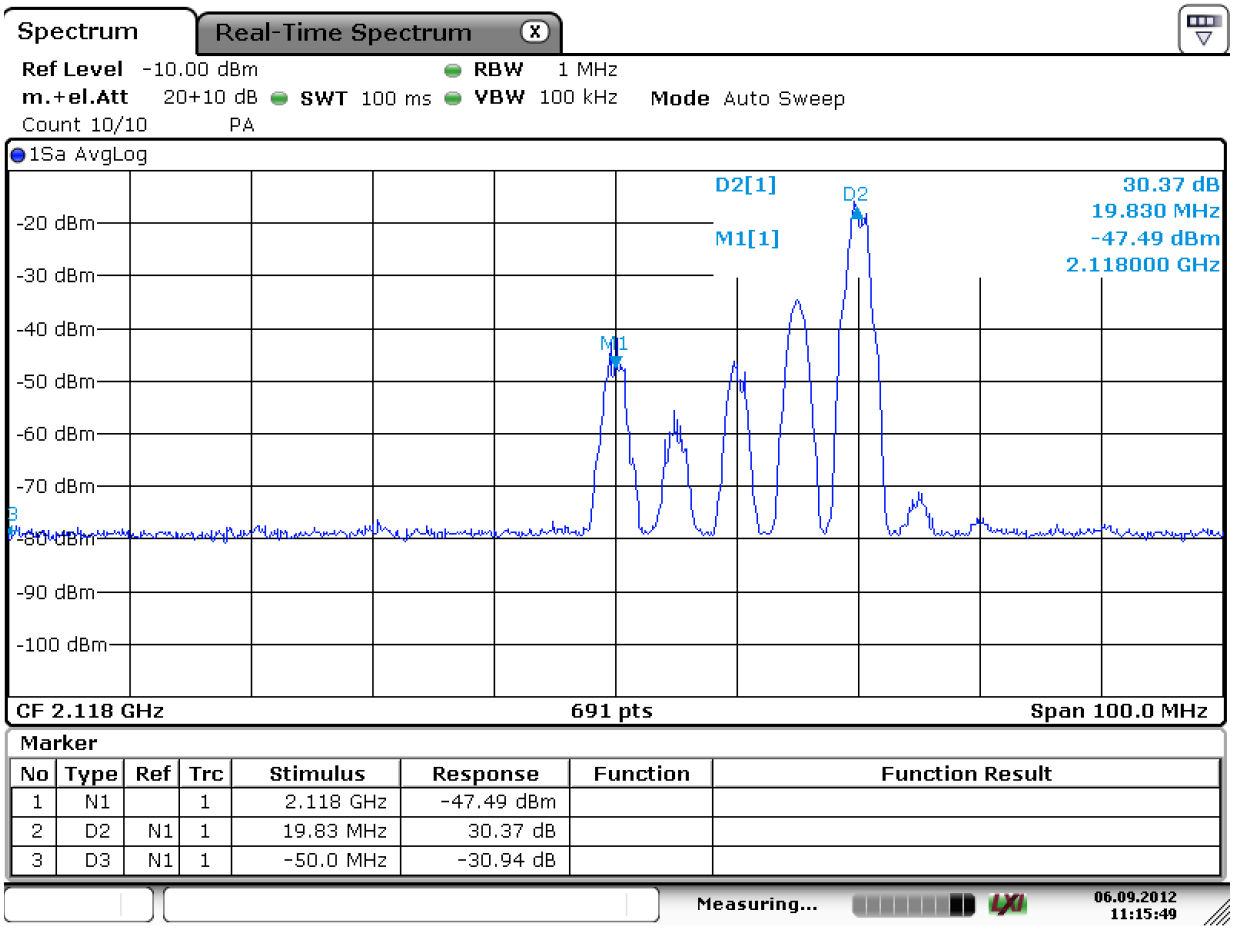

Figure 2-5 Unwanted UMTS band signals

The new TX line-up is shown below.

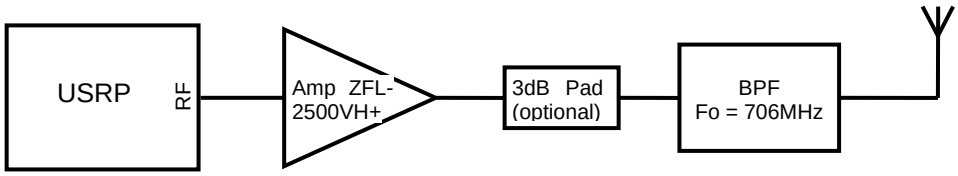

The ZFL-2500VH+ has a P1dB of 25dBm and the filter has an insertion loss of 4dB which together yields a P1dB of 18dBm (25-4-3) in the above circuit. The output power of the TX signal will be backed off depending on the modulation scheme used. In the case of complex modulation schemes with high PAR, this would typically be ≥6dB, so the TX power would be ≤12dBm.

During tests we found that error free reception and range were best when the USRP gain was set to 2; however this is dependent on the complexity of the OFDM-based waveform, the USRP gain setting can be higher. The output power can be increased by 3dB by removing the pad; this would also increase free space range by 41%.

The bandpass filter response is shown in Figure 2-6; the insertion loss is 4dB at 706MHz with a passband of 25MHz. The rejection at 2138MHz, where the highest level TX spurious is emitted, is about 30dB.

The output before and after filtering are shown in Figure 2-7and Figure 2-8 respectively.

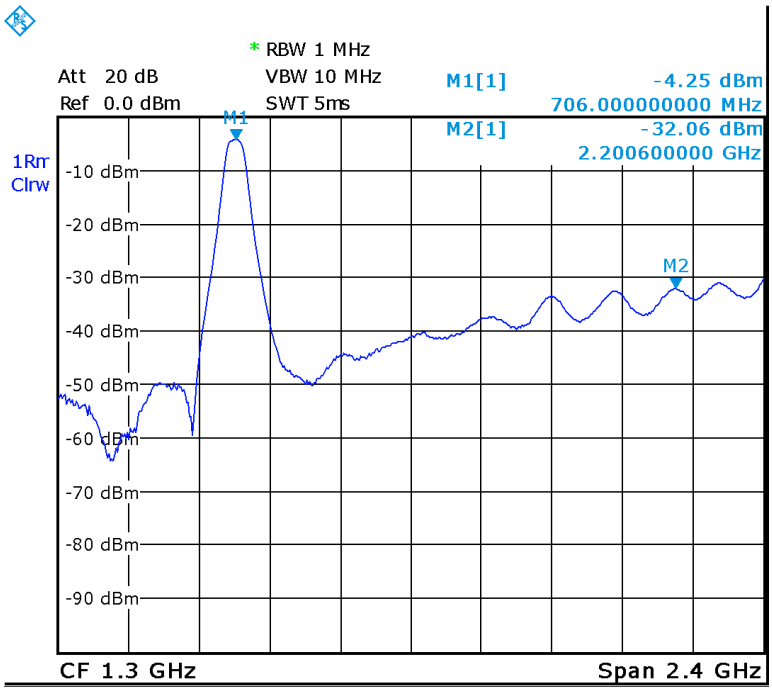

Figure 2-6 TX Bandpass filter response

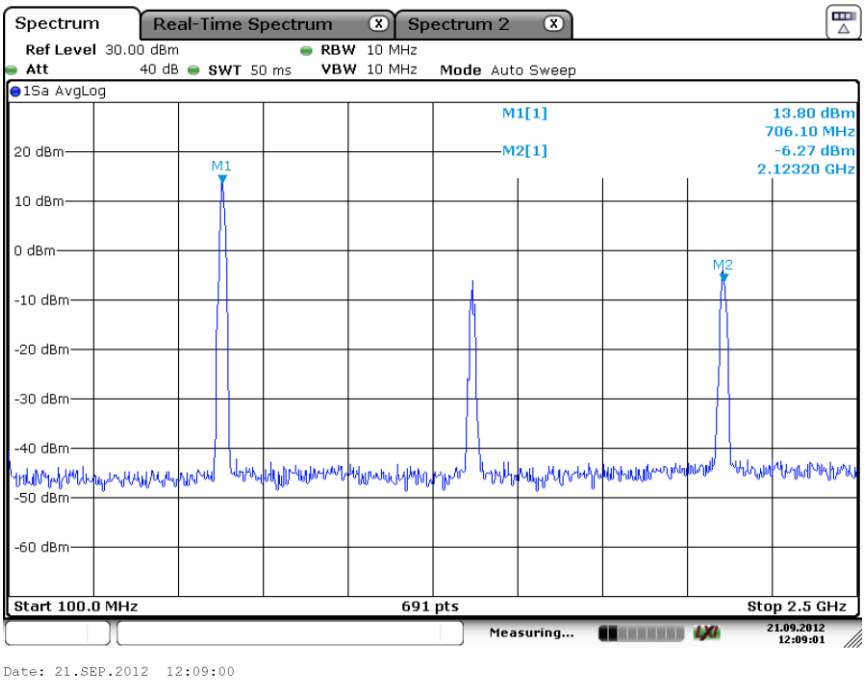

Figure 2-7 TX output without band pass filter

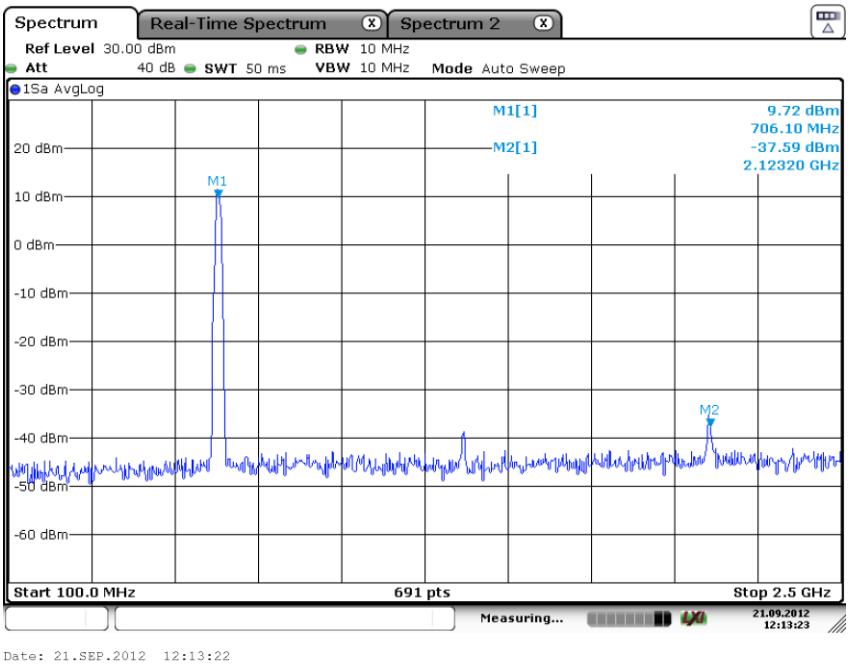

Figure 2-8 TX output with band pass filter

2.3- **Summary**

Inspection of the WBX board indicates that it has a number of spurious emissions located at a number of different frequencies. Given that the WBX was being targeted to the frequency range 694MHz to 718MHz we were able to distinguish between in-band and out of band spurious emissions. The in-band emissions were contained within our band of operation and so were not of concern as we were able to accommodate both the wanted signal and these unwanted emissions within the licenced bandwidth. However, the out-of-band emmissions occurred at a number of frequencies across the range of the WBX board and in particular in the 2GHz UMTS band. A custom-made bandpass filter which addressed these out-of-band emissions was made to address this problem.

In order to achieve an output power approaching the limit of our licensed permission, of 100mW, a COTS amplifier, suited to the frequency range in use, was acquired. This allowed us to operate the WBX on-board amplifier in such a way that it did not distort the transmitted signal. Instead the, approximately 18 dB was achieved using the power amplifier.

3- Spectrum Shaping Evaluation

3.1- Introduction

As described in detail in the previous deliverables from WP5, the COGEU Transceiver implements spectrum shaping techniques that enable to transceiver to exert control over its emissions such that it can co-exist with protected incumbent systems in a safe and efficient manner. It is safe in that it does not interfere with the protected systems. It is efficient in that it uses sophisticated techniques that maximise the in-band power allowed by a given transmit mask that has been designed to protect the incumbents.

The performance evaluation results presented here examine the use of these techniques on the prototype platform under a number of conditions.

3.2- Transmit mask (BEM) compliance and efficiency

For the evaluation of COGEU white space device (WSD) we have chosen a few examples of existing systems spectrum emission masks (SEMs). However, We were limited by the relatively cheap software defined radio platform. As all baseband computations are made on the personal computer equipped with general purpose processor the transmitted signal bandwidth is limited. In general we can say that WSD occupied bandwidth (smaller than sampling rate) can go up to 6-7MHz. Thus we were not able to generate e.g. IEEE 802.11 (18MHz occupied bandwidth) or LTE 10MHz signals. The other limitation is set of available sampling frequencies available for USRP N210. Although a number of them is allowed to be used, only one fourth of them provides steep digital analog filtering. The examples of these sampling frequencies are: 12.5MHz, 8.33MHz, 6.25MHz, 5 MHz, 4.16MHz, 3.57MHz.

The general testbed configuration is:

- Spectrum analyzer: Rohde & Schwarz FSL6
  - Resolution bandwidth: 30kHz
  - Video Bandwidth: 300kHz
  - Trace: averaged over 50- 100 sweeps
  - Attenuation: 15-20dB
  - Center frequency: 540 MHz
  - Frequency span: dependent on mask specification (4-20 MHz)
- Transmitter: IRIS + USRP N210
  - IFFT size (N): 256, 512
  - Cyclic prefix length: N/16
  - Frame structure: 1 OFDM-symbol-length preamble, 32 data OFDM symbols, 1 OFDM-symbol-length empty space
  - WBX board:
    - Gain: 12dB
    - Center frequency: 540MHz
    - Sampling rates: 4,16 or 8,33 Msps

Case 1

The first example is LTE user equipment (UE) SEM for the operation bandwidth of 1.4 MHz [4]. As the subcarrier spacing in LTE is constant (15kHz) this leads us to sampling rates of 1.92 MHz, 3.84 MHz and 7.68 MHz for IFFT sizes of 128, 256 and 512, respectively. The USRP N210 limitations made us to choose two sampling rates 4.16MHz and 8.33MHz, operating using IFFT of size 256 and 512 respectively. It keeps subcarrier spacing close to the LTE system (16.28kHz). For fs=4.16MHz and 8.33 MHz the same indexes of modulated subcarriers were used {-40,.., -1, 1, …., 40}. Although in case of 4.16MHz sampling rate there was no need for additional shaping as frontend filtering fitted the waveform to the SEM (blue curve in Figure 2-9), bigger sampling rate causes the non-shaped waveform to breach SEM (black line in Figure 2-9). Prolonging the OFDM symbol by two samples on each side and multiplication of these regions by Hanning windows allows our signal to keep the SEM (red line in Figure 2-9).

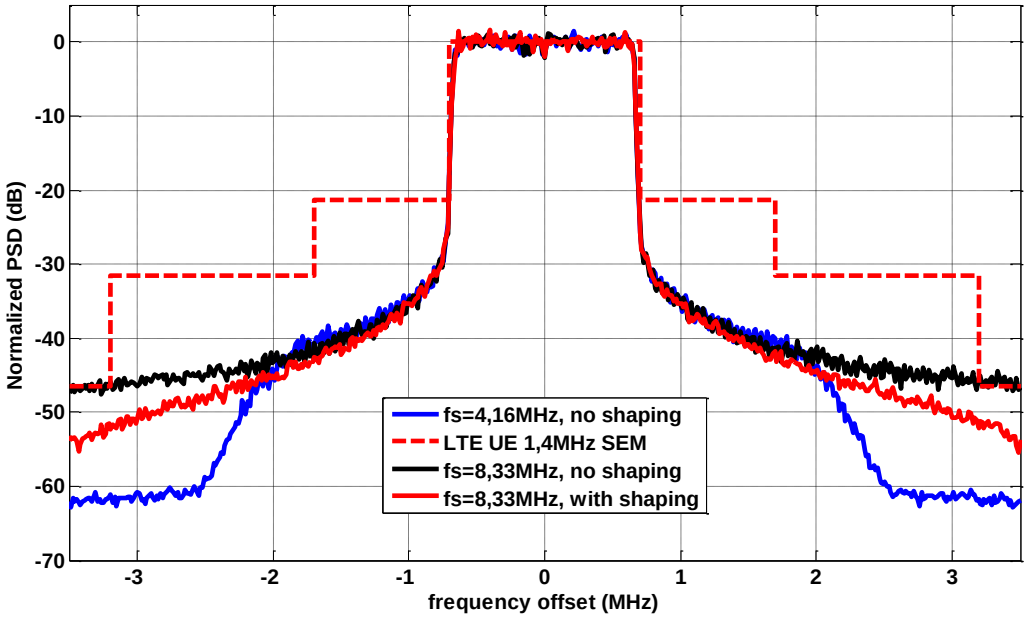

Figure 2-9 PSDs for COGEU TVWS device operating according to LTE UE 1.4 MHz bandwidth standard.

Case 2

The next SEM belongs to 3 MHz bandwidth LTE UE system [4]. For both sampling frequencies (4.16MHz and 8.33MHz, operating with 256 and 512 points IFFT, respectively) the PSDs are well below the prescribed mask as shown in Figure 2-10. The subcarrier indices were {-90,…, -1, 1, …, 90}. In case of lower sampling (blue line) we can observe stepper attenuation of Out-of-Band (OOB) components thanks to narrower digital-analog conversion filter. However, for frequency offset of about 7MHz we observe OOB radiation rise caused probably by some frontend imperfections (e.g. IQ imbalance effects). Fortunately, this rise does not breach the SEM.

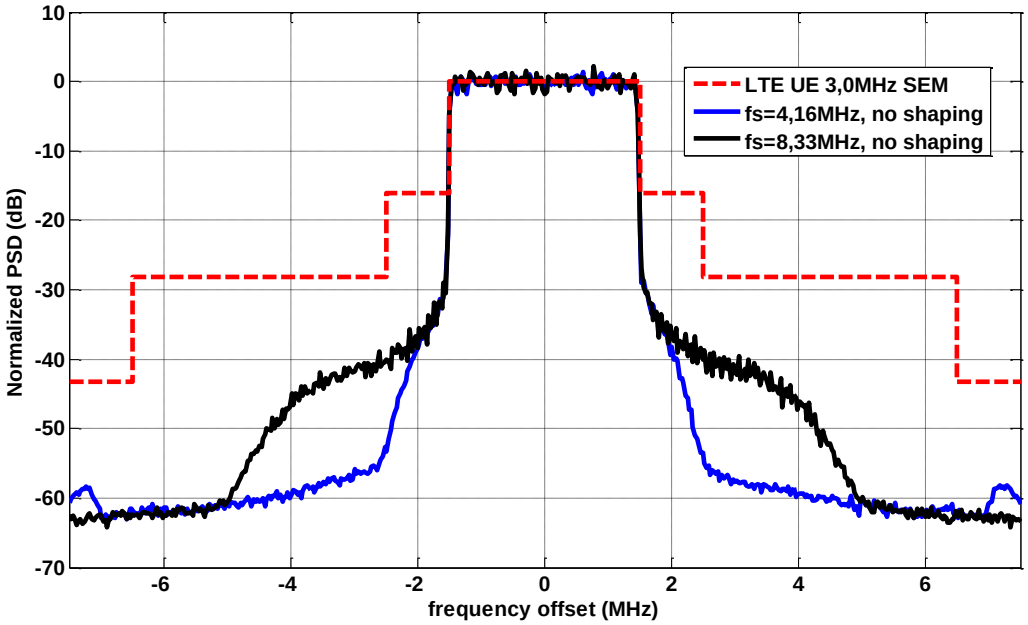

Figure 2-10 PSDs for COGEU TVWS device operating according to LTE UE 3 MHz bandwidth standard.

Case 3

The more demanding is SEM provided for 5 MHz LTE base station taken from Deliverable 3.1 [5]. Here only one sampling rate was tested of 8.33MHz. While IFFT size is 256, our signal occupies subcarriers {-72, …, -1, 1, …, 72}. Although we used 2CCs per edge and 14 samples of windowing extension on each side of OFDM symbol, obtained PSD breaches SEM as depicted in Figure 2-11. As further increase of hanning window length or number of CCs did not bring improvement in PSD plot, that is not observed during computer simulations, we have also depicted in Figure 2-11 noise floor of spectrum analyzer. The reason for breaching the SEM can come from limited dynamic range of spectrum analyzer or nonlinearity of the transmitter frontend.

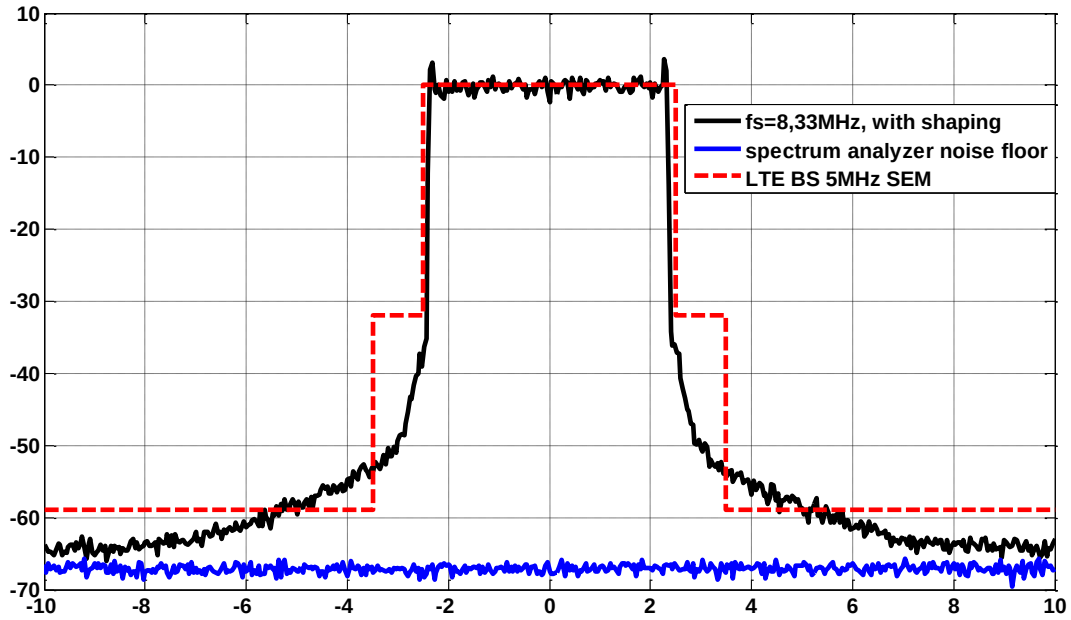

Figure 2-11 PSDs for COGEU TVWS device operating according to LTE BS 5 MHz bandwidth standard.

Case 4

In this case we tried to test our transmitter against FCC rules designed exactly for cognitive devices operating in TVWS [6]. It allows, in case of equal transmit power distribution over 6MHz channel, the adjacent channels to be interfered by at least 55dB weaker OOB radiation (adjacent channel leakage ratio – ACLR). Additionally, the resolution filter bandwidth for evaluation of adjacent band should be 100kHz. Our transmitter operated with sampling rate of 8,33MHz and IFFT size of 256 subcarriers. Occupied subcarriers were {-87,…, -1, 1, 87}. In case of shaping we have used 3 cancellation carriers per subcarriers block edge, and 38 samples of Hanning window on each side of OFDM symbol. The PSDs before and after shaping are shown in Figure 2-12. The shaping provides strong improvement of PSD steepness, but in the region close to occupied channel the OOB radiation reduction is lower than the required 55dB. The reasons can be similar as in Case 3. However, the ACLR measured in the whole 6MHZ channel fits within the FCC regulation (Figure 2-13).

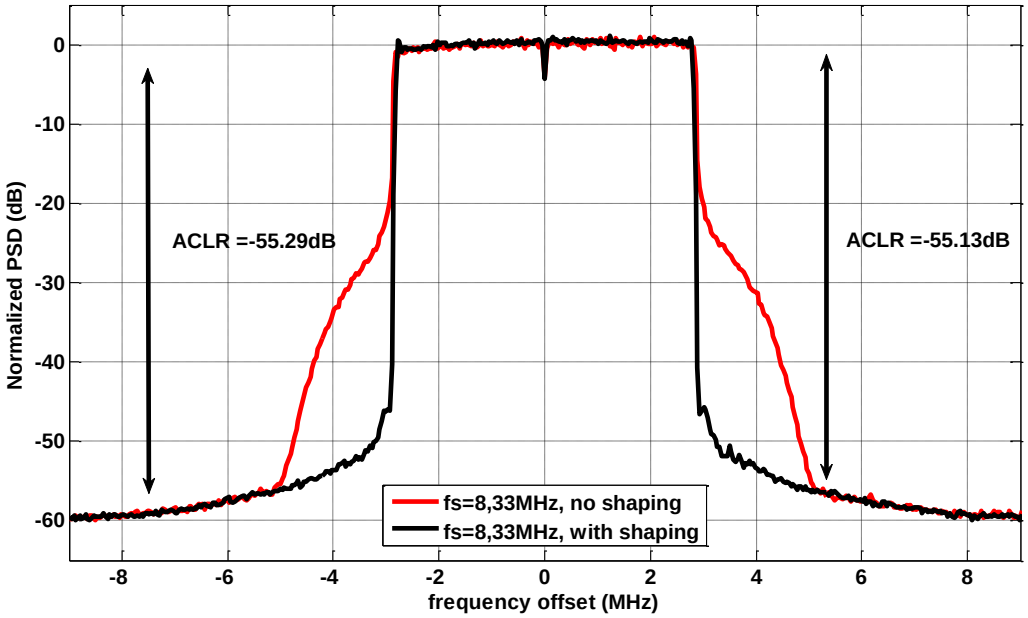

Figure 2-12 PSDs for COGEU TVWS device signals operating according to FCC rules.

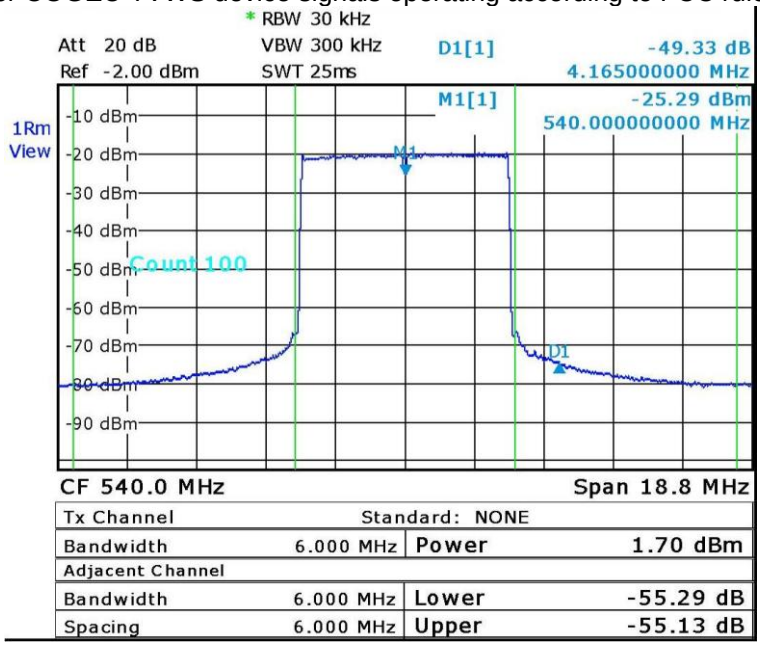

Figure 2-13 PSDs for COGEU TVWS device signals operating according to FCC rules (ACLR measurement).

Case 5

All examples shown above do not make use of the non-contiguous spectrum aggregation feature that is implemented in COGEU WSD. It can be most useful in case of the TV channel occupied only by one narrowband PMSE device (200kHz bandwidth). The example for NC-OFDM transmitter employing 4.16 MHz sampling rate, 256 points IFFT and occupied subcarriers set {-50, …, -1,1, …, 5, 22, …, 50} is shown in Figure 2-14. The system that turns off subcarriers in the spectrum notch (200kHz width) plotted with black line obtains only 20 dB of OOB radiation reduction in comparison to in-band power. Introduction of Hanning window OFDM symbol extension of 14 samples provides OOB radiation components reduction of only few dB in the notch, and about 20 dB in the frequencies more distanced from occupied band (green line). Introduction of only 3 CCs on each subcarriers block edge to non-shaped waveform provides strong OOB radiation reduction in the notch (blue line) while components

more separated in frequency are reduced by a few dB. Combination of both techniques (red line) provides significant OOB components reduction in all OOB regions.

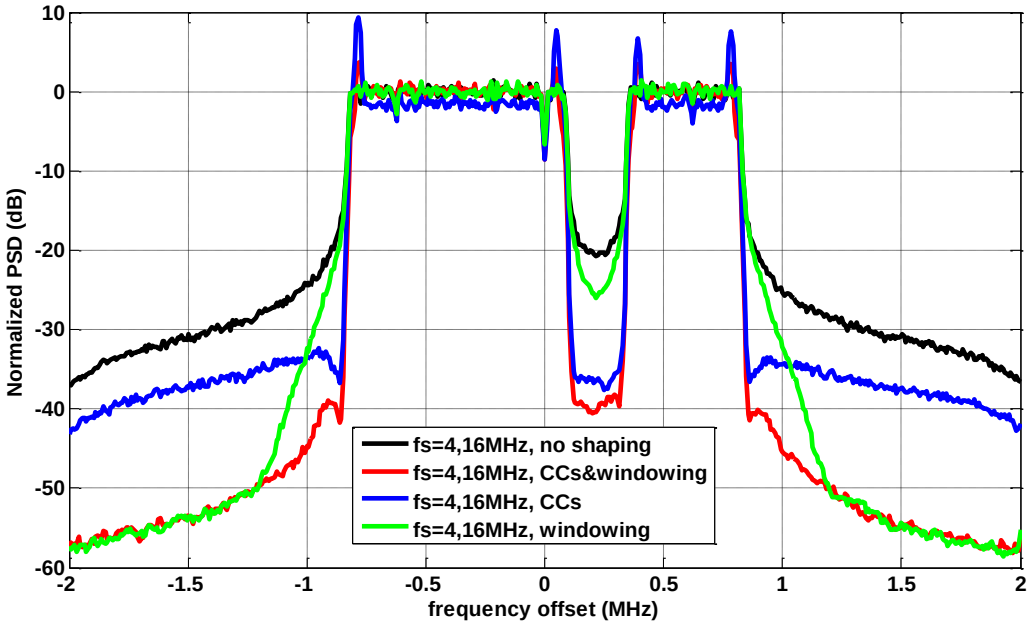

Figure 2-14 PSDs for COGEU TVWS device operating in non-contiguous mode.

3.3- **Link Capacity, QoS**

Spectrum shaping does not have strong impact on reception quality. Bit-error rate is not affected by time domain windowing. Similarly, cancellation carriers are orthogonal to data carriers, so they do not cause intercarrier interference. However, while operating with constant power some of it has to be sacrificed for CCs. If we assume that CCs power is on average the same as data carriers power, the signal to noise ratio (SNR) loss can be calculated as follows:

$$\Delta SNR = 10\log\left(\frac{U-K}{U}\right)$$

where U is number of all occupied subcarriers and K is number of cancellation carriers. On the other hand the use of CCs and time domain windowing lowers the useful link throughput. We can calculate it for each case using following equation:

$$symbolrate = \frac{32 * QAM\_symbols\_per\_OFDM\_symbol}{34 * \frac{1}{\Delta f} * \left(1 + \frac{1}{16} + \frac{extension\_length}{256}\right)}$$

where Δf is subcarrier spacing. For simplicity we do not exclude pilot carriers from QAM_symbols_per_OFDM_symbol, so that the symbol rate is overestimated. However, the error should not be higher than 4%. The results of QAM symbol rate and SNR degradation for all cases investigated in previous subsection are shown in Table 1.

Table 1 Throughput and SNR loss for Case 1-5

	Case 1 fs=		Case 2 fs=		Case 3	Case 4	Case 5
	4.16MHz	8.33MHz	4.16MHz	8.33MHz			
QAM symbols per OFDM symbol (incl. pilots)	80	80	180	180	140	168	72
QAM symbols per frame	2560	2560	5760	5760	4480	5376	2304
Frame duration (μs)	2223	2228	2223	2220	1167	1265	2338
QAM symbols rate (MSps)	1,15	1,149	2,59	2,59	3,84	4,15	0.99
ΔSNR (dB)	0	0	0	0	-0.12	-0.15	-0.67

However, in order to obtain symbol rates listed above successful synchronization in WSD receiver is required. Our synchronization scheme is based on autocorrelation of preamble generated as in [7]. Only subcarriers with even indexes are modulated, that produces in time domain to periods of the same waveform. Although the receiver knows (e.g. thanks to common control channel) before the reception indexes of data carriers, cancellation carriers and length of shaping extension this information is not used on time-domain synchronization phase. As cancellation tones are placed on the edges of data carriers blocks they are usually occupying not only even indexed subcarriers. The cancellation carriers placed on uneven subcarriers will contribute to the self-interference of preamble. If the sum of noise and interference is too high, preventing WSD receiver from obtaining synchronization, we can turn off CCs in the preamble by using "*ifuseccsforpreamble*" parameter in configuration file. Although it will decrease the OOB radiation attenuation for preamble, the other 32 OFDM symbols will be fully shaped. The impact of reduced spectrum shaping capabilities for preamble will be therefore not significant, that was confirmed by means of hardware experimentation.

The more problematic from synchronization point of view is coexistence of the WSD with narrowband PMSE transmission, that is possible e.g. in Case 5. If the frequency modulated PMSE-based signal has low frequency deviation it can be approximated with single tone y(t) transmitted on constant frequency f:

$$y(t) = \exp(-j2\pi f_c t).$$

The autocorrelation of this signal over period T_x is

$$R_{yy}(t_0) = \int_0^{T_x} \exp(-j2\pi f_c (t+t_0) \exp(j2\pi f_c (t+t_0-T_x) dt = \exp(-j2\pi f_c T_x) \int_0^{T_x} 1 dt = T_x \exp(-j2\pi f_c T_x)$$

where t_0 is a starting point of autocorrelation measurement. As the timing metric is normalized over energy contained in the period Tx and absolute value operation is made, the final timing metric equals one. It is independent from the starting point t_0, PMSE carrier frequency f_c or correlation window length T_x. As the correct synchronization threshold is equal 0,827 [7], WSD receiver will obtain false time domain synchronization when PMSE signal is strong enough. During our WSD evaluation process we have tried to measure its resistance to PMSE-based interference. We have made measurements of over the air transmission of NC-OFDM signal transmitted from one COGEU WSD. The center frequency is 539.697MHz and sampling rate is 2.5MHz. Although IFFT size is 256 only subcarriers {-96, …, -1, 1, …, 5, 57, …, 96} are occupied by non-zero values. We did not use CCs but windowing with 10 samples on each side of OFDM symbol was applied. The WSD receiver is configured similarly, but it receives not only NC-OFDM signal, but also PMSE one transmitted on carrier frequency of 540MHz. The example of PSD observed in the WSD receiver is shown in Figure 2-15. In the transmitter the signal power is adjusted to obtain various levels of signal-to-interference ratios (SIR).

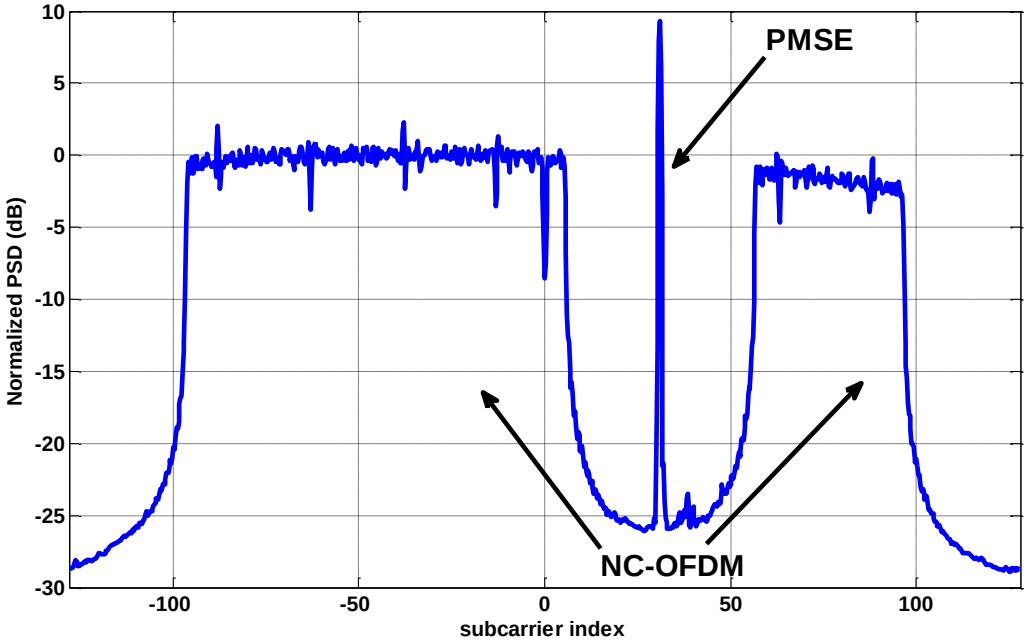

Figure 2-15 Normalized PSD of signal received in WSD receiver.

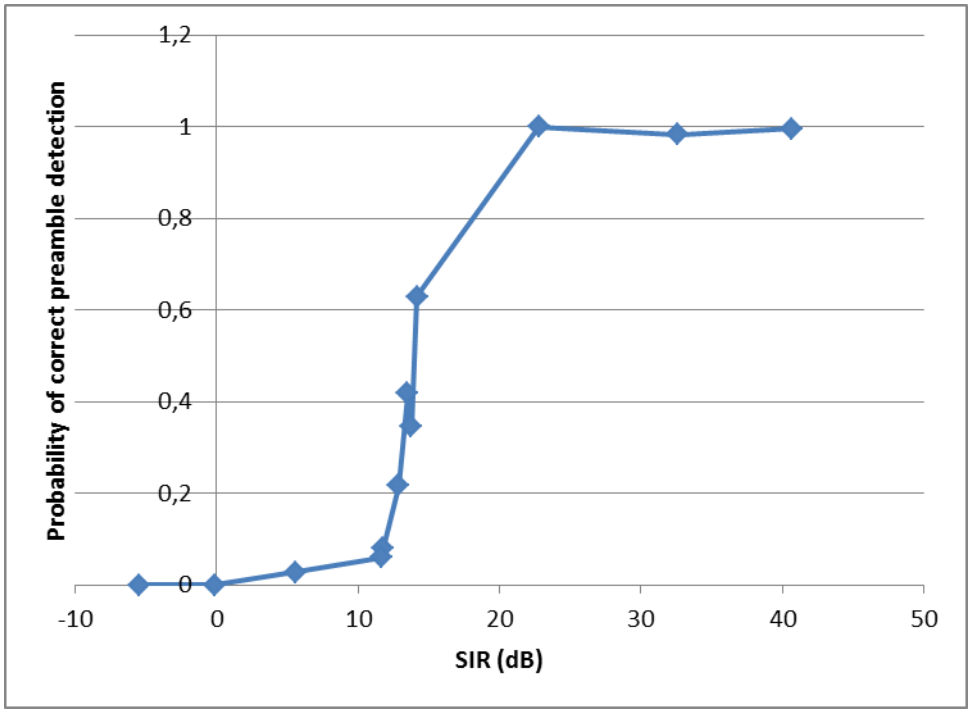

Figure 2-16 Probability of correct preamble detection for NC-OFDM transmission interfered by PMSE device.

The results are presented in Figure 2-16 as probability of correct preamble detection in the function of SIR. It is visible that the SIR has to be higher than 14dB to detect correctly 60% of preambles. As these measurements were made over the air, the accuracy of result might be quite poor. Additionally we do not take into account the noise level (we tried to make it negligibly low in comparison to interference) and possible changes of WSD parameters. Though, these results show us an important phenomenon that can affect WSD link quality and approximate SIR required for correct preamble detection. As it was mentioned before, the other stages of NC-OFDM signal reception are carried in frequency domain where the interference does not have strong influence on data carriers.

3.4- Impact of WSD operation on PMSE devices

Spectrum shaping was introduced into WSD as cognitive radio has to provide protection of primary users. We decided to check the protection of PMSE device not only on PSD plot (as it depends on averaging, resolution bandwidth etc.) but also by means of sound quality evaluation. We have set up following test environment:

- WSD transmitter operating in TV band
  - USRP N210 +WBX board
  - Center frequency: 532,7MHz
  - Sampling rate: 3,846Msps
  - IFFT size: 256 points
  - CP length: 16 samples
  - Configuration of spectrum shaping and data carriers: Table 2
- PMSE transmitter: AKG PT45 (analog instrumental set, connected to mp3 player for transmission of known sound)
  - Carrier frequency: 532,7MHz
- PMSE receiver: AKG SR45 (analog receiver, connected to PC computer for received sound recording)
  - Carrier frequency: 532,7MHz
- Spectrum analyzer: Rohde & Schwarz FSL v6 – antenna placed close to PMSE receiver to get estimate of primary to secondary user power ratio (P_{PU}/P_{SU}) on PMSE receiver antenna (we do not have access to RF frontend of PMSE receiver).

Table 2 Parameters of test cases for PMSE protection evaluation

Test case	Data carriers	Spectrum shaping	Relative NC-OFDM OOB radiation attenuation in PMSE band
Contiguous OFDM	{-100,…,-1,1,…,100}	-	0dB
NC-OFDM, narrow notch, no shaping	{-100,…,-8,8,…,100}	-	-17.85dB
NC-OFDM, wide notch, no shaping	{-100,…,-18,18,…,100}	-	-22.7dB
NC-OFDM, narrow notch, shaping	{-98,…,-10,10,…,98}	2CC per edge, 10 samples of window extension	-30dB

In the Table 2 we can see for each NC-OFDM configuration mean OOB radiation attenuation (relative to in-band power) of NC-OFDM transmitter measured in PMSE band (200kHz bandwidth). These values were calculated using PSDs plots presented in Figure 2-17.

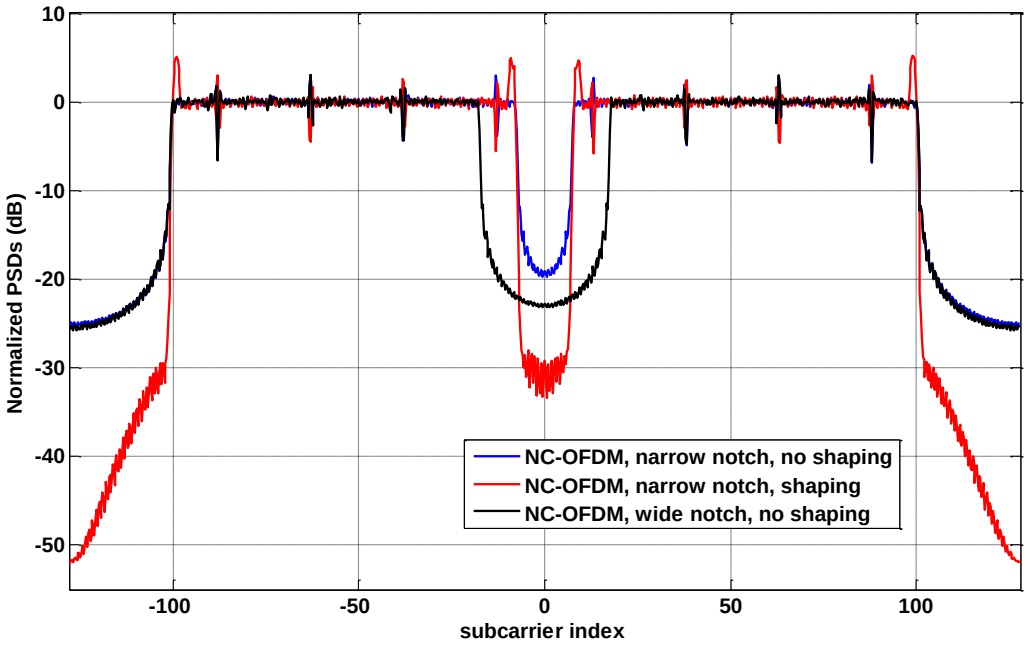

Figure 2-17 PSDs plots of signals used for evaluation of influence of NC-OFDM based interference on PMSE sound quality.

The sound quality for each test case was obtained by comparing reference sound to the one recorded while operating under interference from NC-OFDM transmitter. The sound quality metric is Signal-to-noise and distortion ratio (SINAD) that is calculated as the ratio of whole received sound power to the power of signal after extraction of wanted signal. It is commonly used for the measurement of sound quality, e.g. [8]. In the same document the minimum value of SINAD for PMSE devices is chosen to be 30dB. However, according to our testing procedure and SINAD measurements the limit of 25dB SINAD can be stated that provides sound without any audible distortions.

The results of SINAD for varying ratios of P_{PU}/P_{SU} (note: not signal to interference ratio, as it will have to be measured after reception filter of PMSE device) for all test cases is presented in Figure 2-18. The P_{PU}/P_{SU} ratio was changed by alteration of transmit power of NC-OFDM transmitter. It is visible that for typical contiguous OFDM, SINAD of 25 dB is obtained when primary transmission is 15 dB stronger than the secondary transmission. We can increase secondary power by about 13dB after turning off 14 subcarriers in the PMSE band while obtaining the same sound quality in the PMSE link. Additional 3dB of increase can be get by increasing spectrum notch width. However, such a solution is spectrally inefficient. High spectral efficiency combined with allowed secondary user power higher by 21 dB in comparison to contiguous OFDM case can be obtained while operating using NC-OFDM with narrow notch and shaping algorithms employed. It proves that the spectrum shaping algorithm developed in COGEU project has direct impact on protection of primary users. Thanks to its utilization we can increase allowed transmission power of secondary user while providing the same level of its protection.

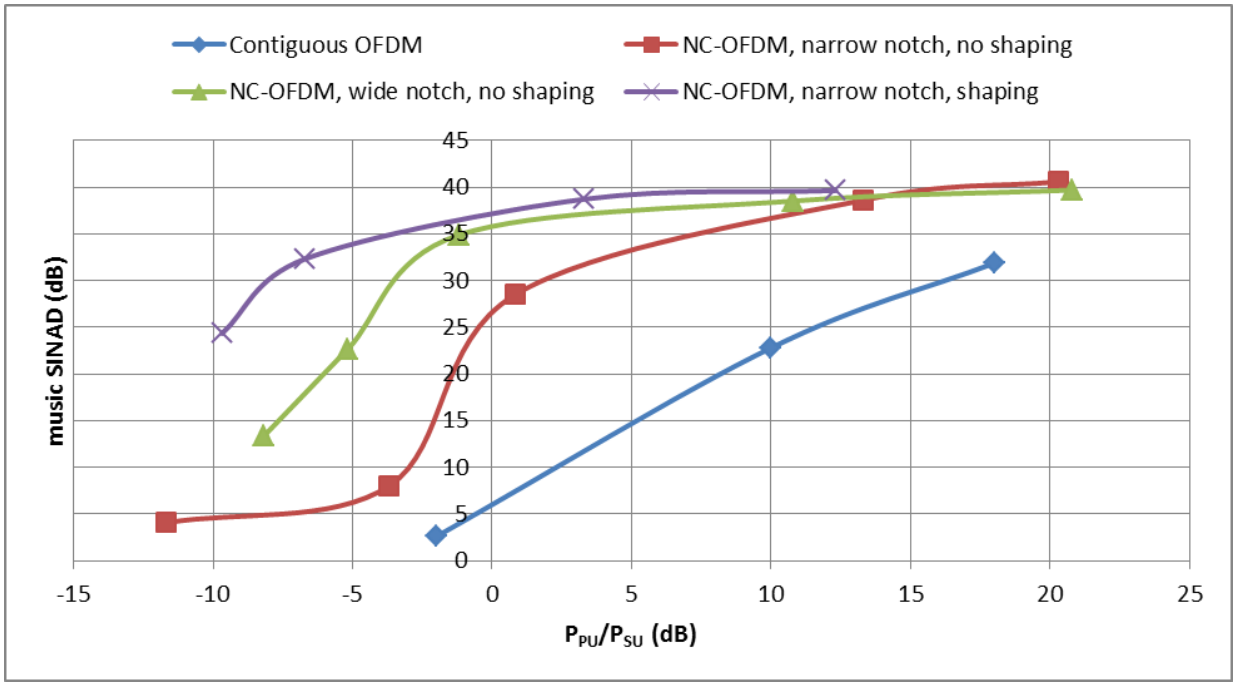

Figure 2-18 SINAD of music received in the PMSE receiver in function of primary to secondary user powers ratio.

3.5- **Summary**

A number of conclusions can be drawn from the work presented here:

- Spectrum shaping mechanisms work efficiently under certain limitations caused by USRP frontend (intermodulations, only some sampling frequencies allowed), and PC (computational complexity).
- The link capacity is only slightly dependent on spectrum shaping algorithms (throughput decrease because of CCs and windowing introduction, SNR loss negligible).
- Time domain synchronization can be disturbed by CCs (we can turn them off only in the preamble) and interference from primary systems. Efficient synchronization strategy under strong interference from primary devices is required. For now we need 20 dB SIR for correct transmission in the presence of PMSE device.
- Spectrum shaping gives improvement not only on PSD plot, but also for end user QoS experience. With the same spectrum occupation (narrow notch) we can increase secondary user power by e.g. 8 dB providing the same sound quality to PMSE device user.

4- Rendezvous Evaluation

4.1- Introduction

Rendezvous is used the TVWS system to enable the master and slave TVWS devices to communicate in unchannelised spectrum using intentionally embedded cyclostationary signatures. The motivation for the use of this technique was presented in D5.2 [1]. The implementation and integration and this component was described in D5.3 [2]. The Rendezvous component has been implemented as a sub-component of the OFDM modulator and demodulator components in the COGEU TVWS Transceiver.

The performance of the Rendezvous technique depends on the ability of the detector situated at the receiver to accurately and quickly detect the presence of Cyclostationary signatures that are embedded in a waveform.

As previously described in detail in Deliverable 5.2, Cyclostationary signatures can be easily embedded in multicarrier waveforms through subcarrier mapping. This process involves the transmission of identical data symbols on two discrete sets of subcarriers and is illustrated in Figure 4-1 for an Orthogonal Frequency Division Multiplex (OFDM) signal. Here, F_0 is the DC carrier, B_{sig} is the signal bandwidth and p is the subcarrier set separation. The size of the subcarrier mapping, M, is 4 in the case of the example depicted in the figure.

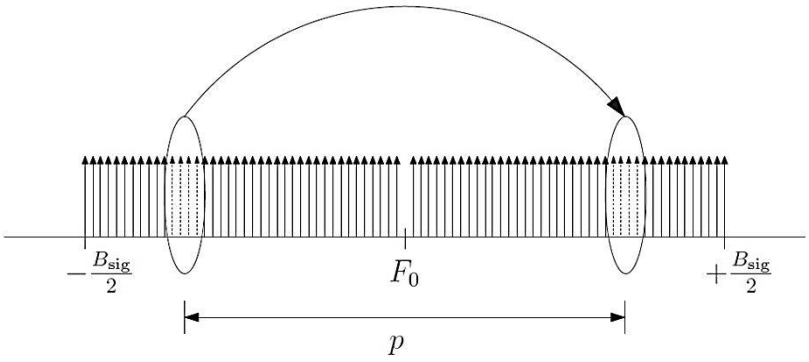

Figure 4-1 Generation of a Cyclostationary Signature using OFDM Subcarrier Set mapping

It was shown, through simulation, that Rendezvous provides robust mechanisms for two radios to establish communication under quite harsh radio conditions. As implemented in the TVWS prototype, Rendezvous enables the assignment of spectrum between master and slave nodes in the TVWS spectrum allocated to the master by the Broker or Geolocation database.

In the following subsections we present a series of experiments which evaluate the performance envelope of the cyclostationary signature technique. The first set of experiments evaluate the performance of the detector with regard to its Time To Rendezvous (TTR) characteristics. These experiments enable us to understand where the optimal range for the number of mapped subcarriers used in an individual unique feature with regard to the observation time allowed at the receiver.

In the second set of experiments we investigate the reliability of the detector. Specifically, we report on the Probability of detection P(det) and Probability of false alarm P(fa) statistics for the detector under a number of scenarios.

4.1.1- Experimental evaluation set-up

The set-up comprised of a transmitter and a receiver operating in an indoor laboratory setting. The transmitter and receiver were both comprised of PCs operating the Iris software radio connected to USRP N210s fitted with WBX RF daughterboards. Details of Iris and the USRPs were given in D5.1 [3].

The experiments were undertaken at 706MHz, within the frequency band of 694MHz to 718MHz assigned to CTVR, Trinity College Dublin for experimental purposes by the Irish spectrum regulator.

All of the experiments that were carried out were static, i.e. none of the elements of the experiment were mobile. As the simulations detailed in Section 4.6 of D5.2 indicate, for mobility to have a bearing on the performance of the Rendezvous technique operating at these TV Band frequencies, the speed of the receiver would need to approach 150km/h, something which is clearly impractical in a low-power laboratory setting.

4.2- **Time-To-Rendezvous**

In these experiments we examined the detector's performance with regard to Time To Rendezvous (TTR). We varied two parameters which are under the control of the TVWS; the size of the signature used, i.e. the number of subcarriers that are mapped, and the length of the observation time.

The number of averaging windows essentially represents the observation time of the detector, relative to the size of the FFT used. In order to perform a Cyclostationary analysis of a particular band, the detector takes in a number of samples (size of FFT) and performs an FFT of the samples. The detector then shifts the window and compares it with itself (Cyclostationary signature detection). (See Section 4.4 of Deliverable 5.2 for more details.) The number of windows used represents the number of times this action is performed and averaged.

In addition to varying the window size and the number of mapped subcarriers used, *M*, we also varied the burstiness of the signal with respect to the presence of the embedded signature. This was done to test the robustness of the detector to signals in which, for whatever reason, a signature is not constantly transmitted. It should be recalled that the Rendezvous technique is only used to detect the initial presence of a signal of interest in a bandwidth of interest to the receiver. Once the receiver has detected its master's signature it can continue to demodulate the signal and bootstrap itself to the network using other means. As such, the only critical time for a signature to be present in a consistent manner is when a slave node is trying to initially rendezvous. In the experiments that follow we experimented with signals which have an embedded signature duty cycle of 100%, 80% and 60%.

Figure 4-2 to Figure 4-5 show the results of experiments carried out at 706 MHz for cyclostationary signatures containing 2, 4, 6 or 8 mapped subcarriers, i.e. where M = 2, 4, 6 or 8. The receive power, as measured at the receiver, for each of these experiments was -75dBm. Each graph contains 3 sets of data points; one for signals with a constant signature presence, i.e. the red data series for DC = 100%, and one each for a DC = 80% (green data) and DC = 60% (blue data). The window size in each of these experiments was varied from 5 to 80, with a concentration of experiments in the area of interest, discussed later.

For every iteration of the experiment, i.e. each data point on each graph, the average result of 50 runs of each experiment are presented. Figure 4-6 to Figure 4-9 show the results of experiments carried out at a weaker receive power of -85dBm. Again, these are carried out at 706 MHz for cyclostationary signatures containing 2, 4, 6 or 8 mapped subcarriers, i.e. where M = 2, 4, 6 or 8.

4.2.1- **Graphs of TTR experiments at -75dBm receive power, 706MHz**

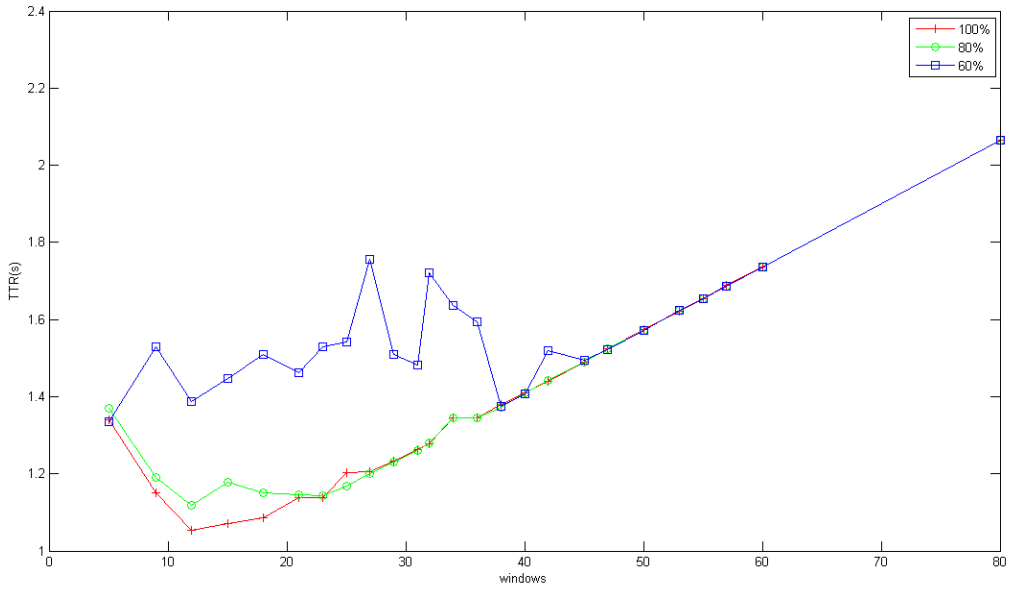

Figure 4-2 TTR: 706Mhz, -75dBm, 8 subcarrier signatures

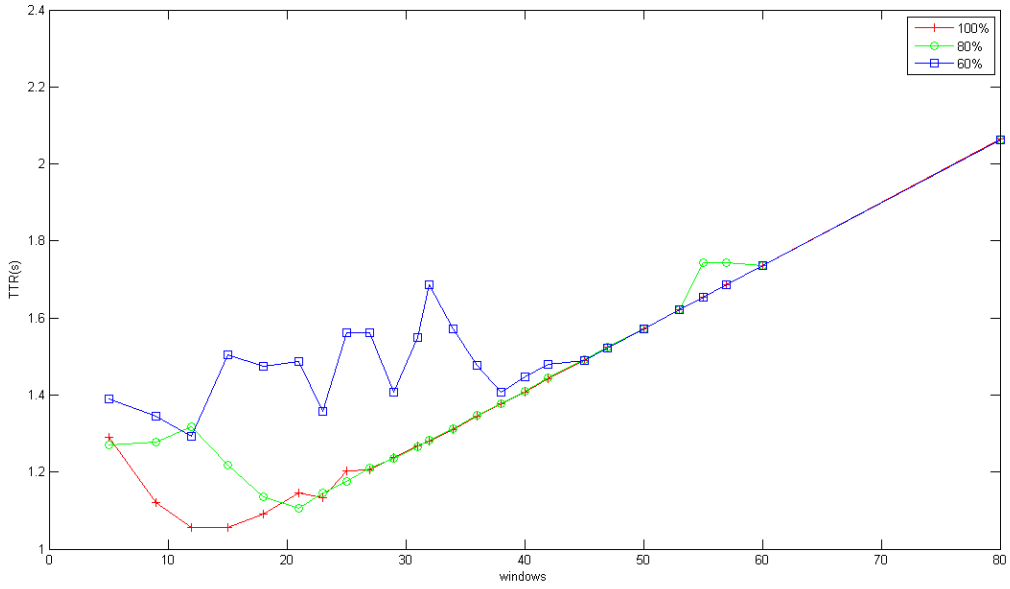

Figure 4-3 TTR: 706Mhz, -75dBm, 6 subcarrier signatures

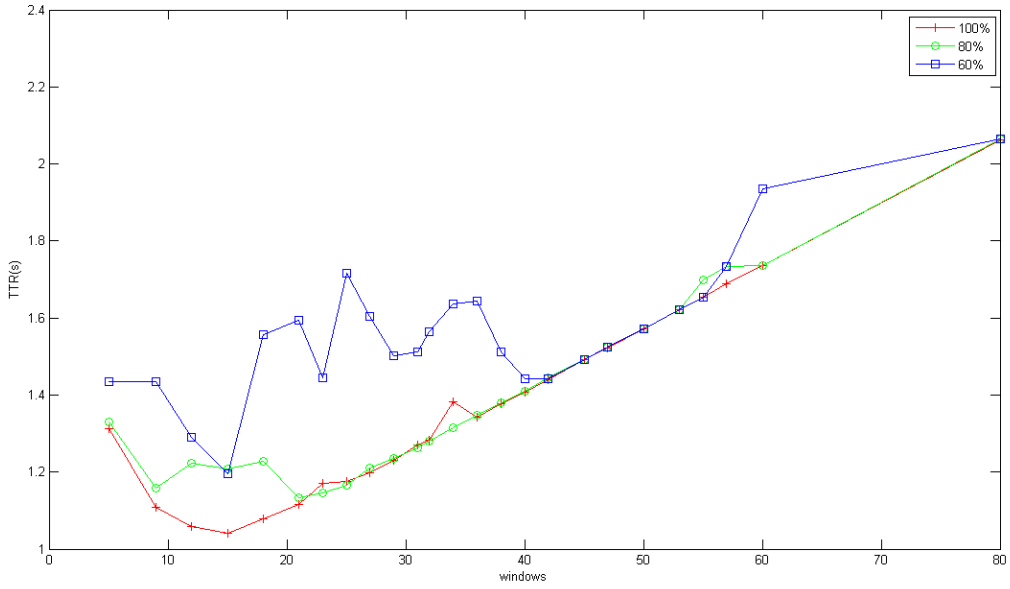

Figure 4-4 TTR: 706Mhz, -75dBm, 4 subcarrier signatures

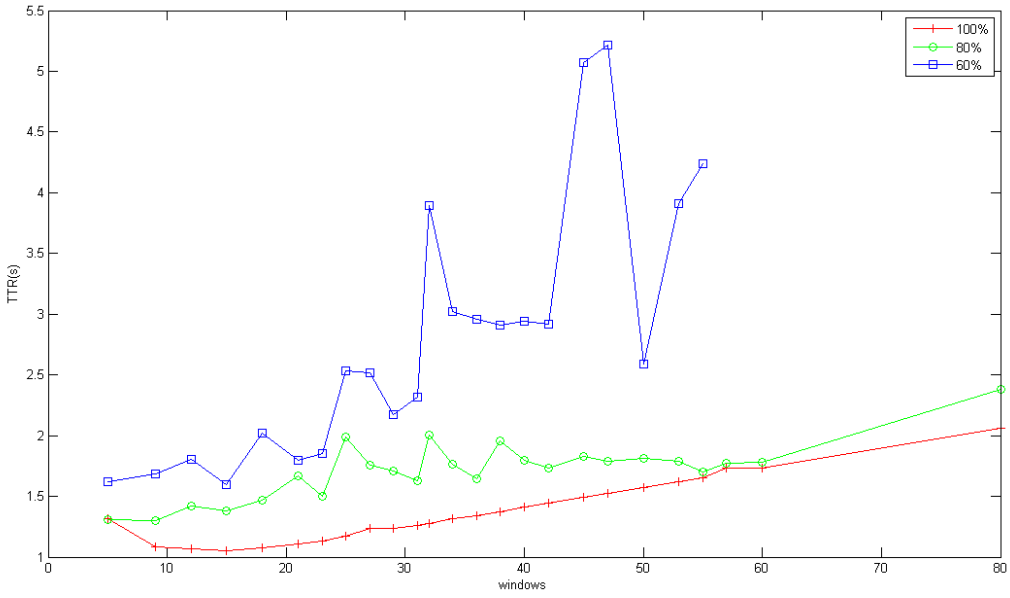

Figure 4-5 TTR: 706Mhz, -75dBm, 2 subcarrier signatures

4.2.2- **Graphs of TTR experiments at -85dBm receive power, 706MHz**

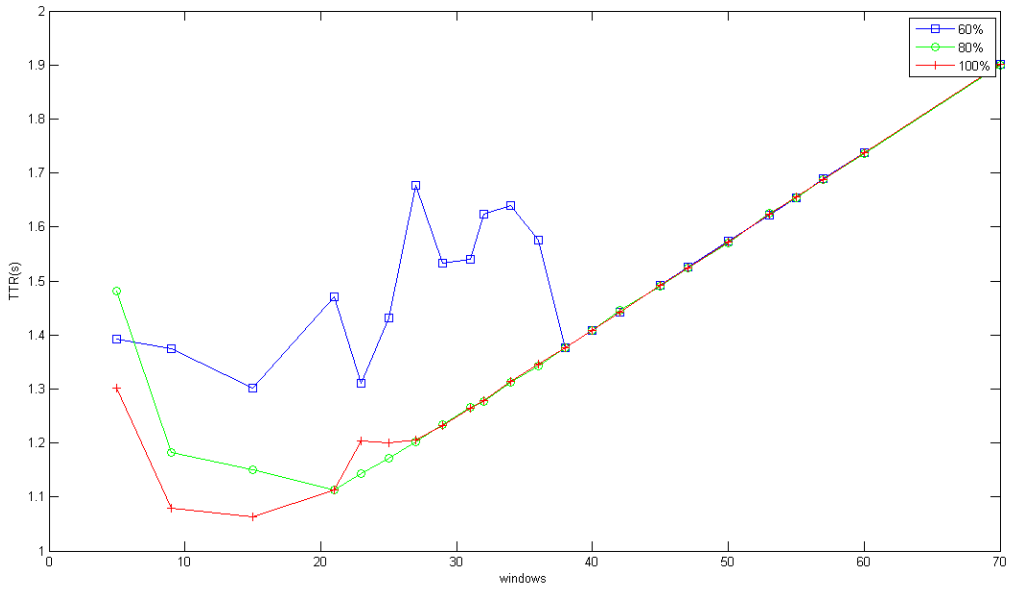

Figure 4-6 TTR: 706Mhz, -85dBm, 8 subcarrier signatures

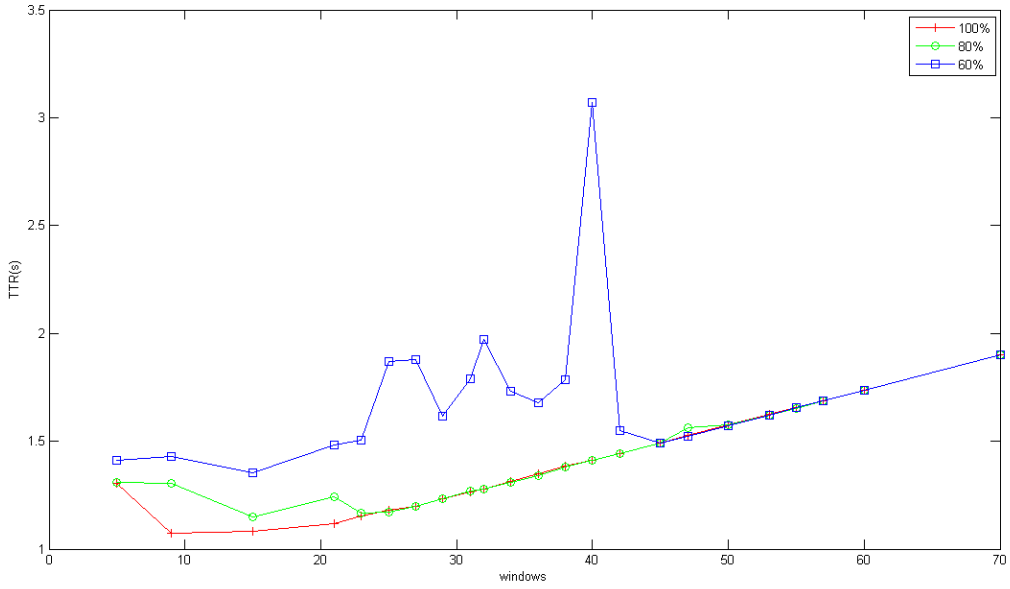

Figure 4-7 TTR: 706Mhz, -85dBm, 6 subcarrier signatures

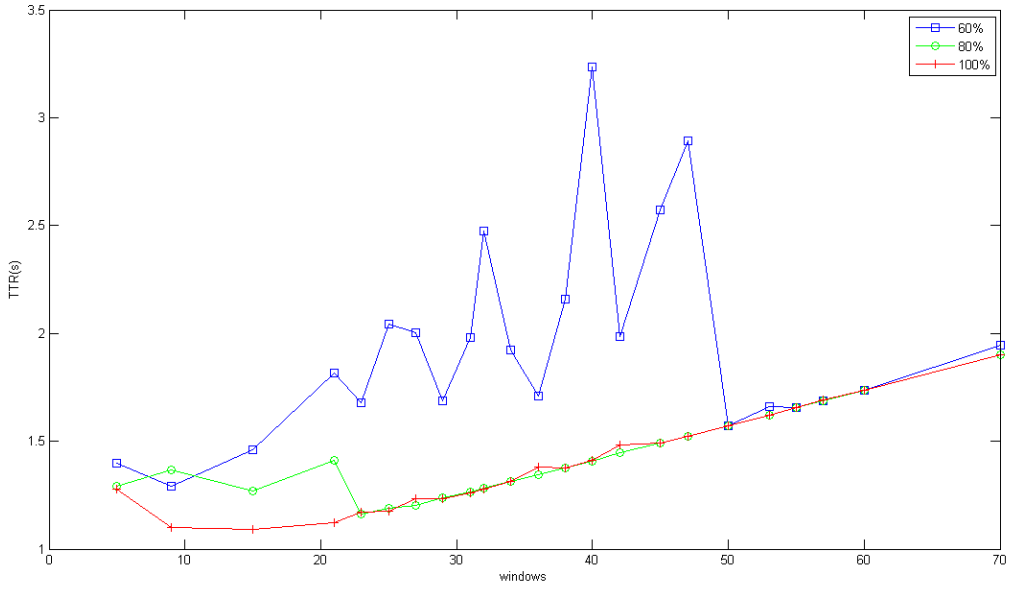

Figure 4-8 TTR: 706Mhz, -85dBm, 4 subcarrier signatures

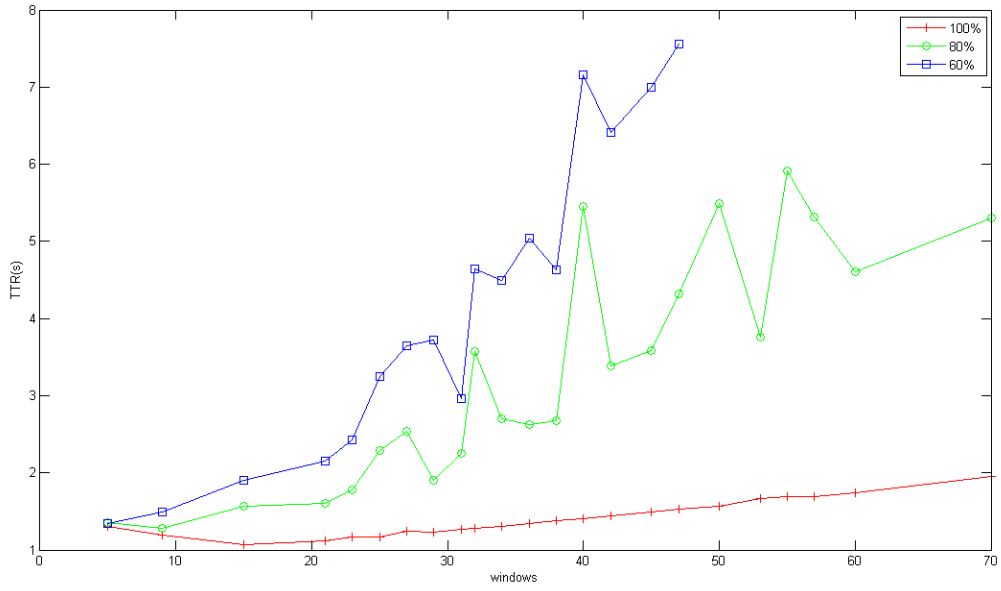

Figure 4-9 TTR: 706Mhz, -85dBm, 2 subcarrier signatures

4.2.3- **Discussion of TTR performance results**

As can be seen in the TTR results, presented here, generally the more windows used by the detector the longer the detection process takes and hence the longer it takes for the receiver to rendezvous with the transmission. However, there are a number of interesting observations that can be made about the optimal areas of operation of the detector.

For the case of signals where there is a constant presence of the signature, i.e. the signature is non-bursty in nature, then we can observe that there is an optimal range within which to set the window size.

Looking at Figure 4-2, the area of interest is between 5 and 30 windows for the red data series, i.e. DC = 100%. When the observation window is 5, the TTR is 1.34s. As the window size increases the TTR

drops until it reaches a minimum of 1.053s at 12 windows. After this point and as the window size increases again, the TTR increases. At 29 windows, the TTR is back up to 1.29s. The reason for the detectors slower performance between a window size of 5 and 12 is that the detector has not been able to make enough observations to detect the presence of the signature above the required decision threshold. However, for any further observations beyond 12 windows the larger window size serves only to delay the detector's TTR. It can be seen that the detector's TTR performance degrades linearly with increasing window size once it leaves the minimum.

For each of the scenarios graphed in Figure 4-2 to Figure 4-5 it can be seen that the optimal window size range for a constant signature is between 12 and 20. This same performance profile is repeated for the other experiments where the signature has a constant presence.

We also observe that the signature size has little effect on the TTR. For the case where the number of mapped subcarriers is 8 or 6, the smallest TTR is given by an observation window of 12, whereas when the signature is weakened to 4 or 2 mapped subcarriers, the TTR is at a minimum for a window size of 15.

However, when the transmission becomes bursty, i.e. when the effective duty cycle of the signal carrying embedded signatures is less than 1, the TTR becomes nonlinear with the number of windows. We can see from many of the graphs that for the region between 5 and 22 windows for an 80% duty cycle and between 5 and 40 windows for a 60% duty cycle, the detector displays this non-linearity. This can be explained by the size of the observation period becoming a size such that landing on the 'off' period of the duty cycle can cause the detector to calculate a correlation level below the set threshold level.

This can be expressed by the following formula:

$$(2)*(numWindows)*(FFT) >> (1/1-threshold)*frame\_size*(1-DC)$$

The left represents the receiver observation time, the 2 accounts for the fact that the transmission is at double the bandwidth of the receiver (half the subcarriers are nulled to counteract the filter cutoff at the receiver. This is an artefact of the hardware used.). *numWindows* * FFT accounts for the total number of samples read in one detection.

The right represents the minimum window size that will be guaranteed to fit the full 'off' section of the duty cycle as well as enough of the 'on' section of the duty cycle to ensure the threshold is reached by the detector.

So, for the case of a detection with *numWindows* = 40, FFT = 1024, *threshold* = 0.3, *frame_size* = 12,672, DC = 0.6:

2*40*1024 = 71680

1/1-0.3*12672*4 = 72411

Since the left side is smaller than the minimum observation time it is possible for the observation period to land on a section of the duty cycle that will give a false negative detection.

The combined effects of the burstiness and smaller signatures can be seen in more extreme cases in Figure 4-5 and Figure 4-9. In both of these graphs, while the detector works well for a constant signature presence it becomes erratic as duty cycle is reduced. It should be noted that the detector does ultimately detect the presence of the signature in each case; it is simply that the bound on its performance is not as predictable, or tight. In order to guarantee a linear, and predictable, detector performance, the window size should be chosen such that it lies in an area that, when combined with the burstiness of the signal, gives a certain guarantee of performance.

4.3- **Reliability of the Detector**

A further series of experiments were undertaken to evaluate the reliability of the COGEU TVWS device. These experiments set out the Probability of detection P(det) and Probability of false alarm P(fa) statistics for a number of scenarios.

The reliability of the detector can be tuned by the radio designer by setting certain parameters; the number of averaging windows used in the Rendezvous detector and the threshold used. As power normalization is performed at the detector using the autocoherence function, threshold levels are set in the range [0,1] as described in Section 4.4 of D5.2. This threshold is set by the radio designer according to the requirements of the current application.

A series of experiments were undertaken to evaluate the performance of the detector and graphs of the results are shown in the following subsections. Each graph contains data series for Probability of detection P(det) and Probability of false alarm P(fa). The Probability of detection P(det) data is given for signals in which a signature has been embedded; in these experiments signatures with 8 subcarriers and 4 subcarriers are used. Again, as with the TTR experiments described in Section 4.2, we experimented with signals where the embedded signature is not always present, i.e. the signature DC is less than 1. Specifically, they were run for DC = 100%, 80% and 60%.

The Probability of false alarm P(fa) figures were obtained by running experiments where a signal was transmitted with no signatures embedded.

All experiments were run for 3 threshold levels; 0.3, 0.4 and 0.5. They were all also run for varying observation window sizes, ranging from 4 to 100.

The experiments were also run for scenarios where the receive power was set at -75dBm and -85dBm.

4.3.1- **Graphs of reliability experiments with 8 subcarrier signatures, -75dBm**

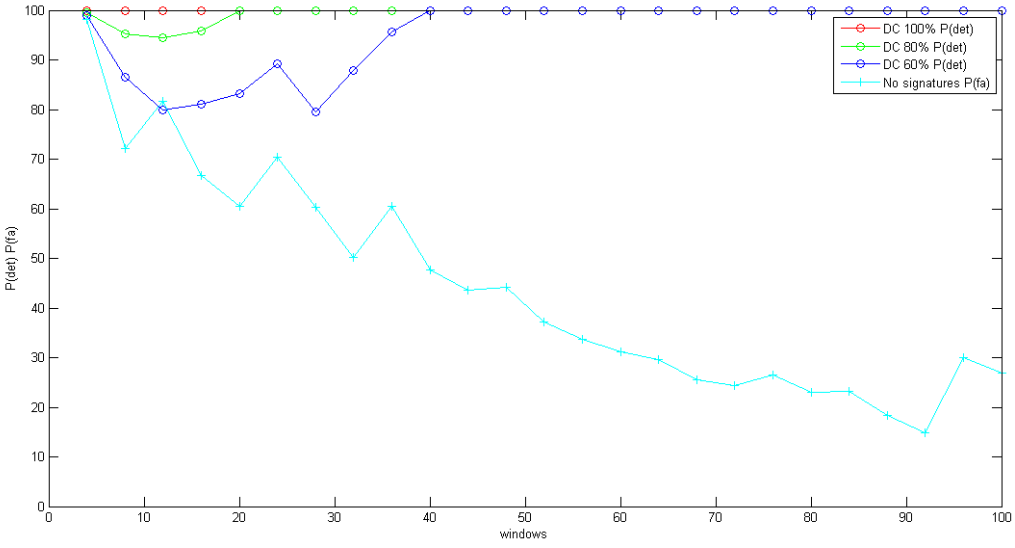

Figure 4-10 Reliability: 8 subcarrier sig, threshold 0.3, receive power -75dBm

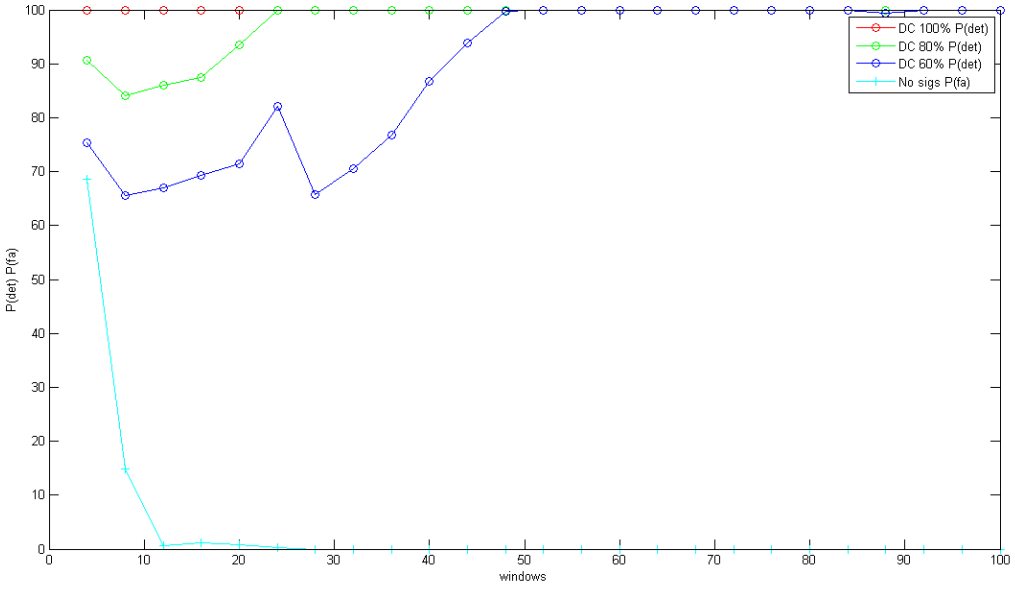

Figure 4-11 Reliability: 8 subcarrier sig, threshold 0.4, receive power -75dBm

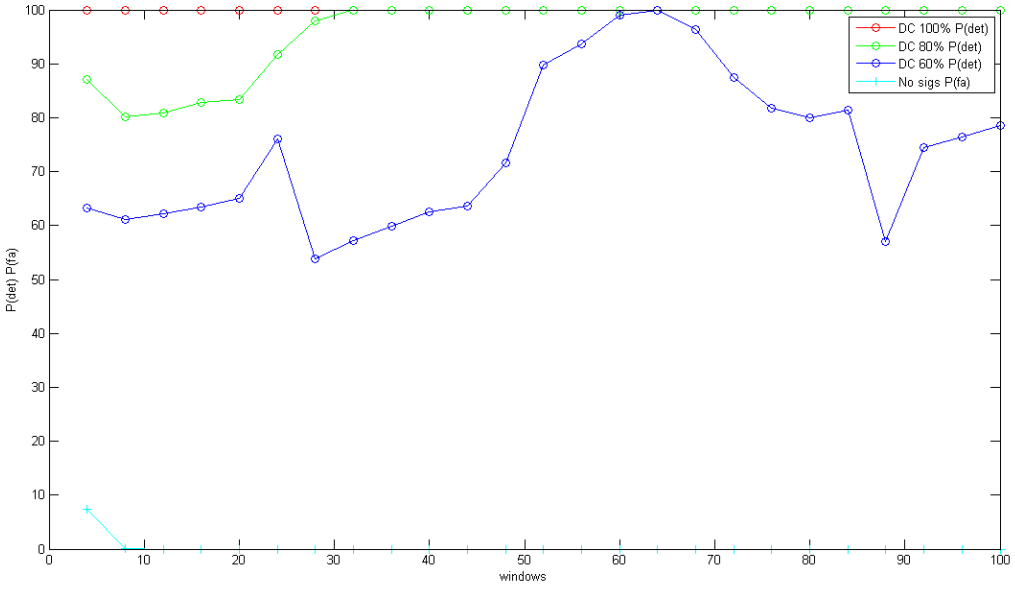

Figure 4-12 Reliability: 8 subcarrier sig, threshold 0.5, receive power -75dBm

4.3.2- **Graphs of reliability experiments with 8 subcarrier signatures, -85dBm**

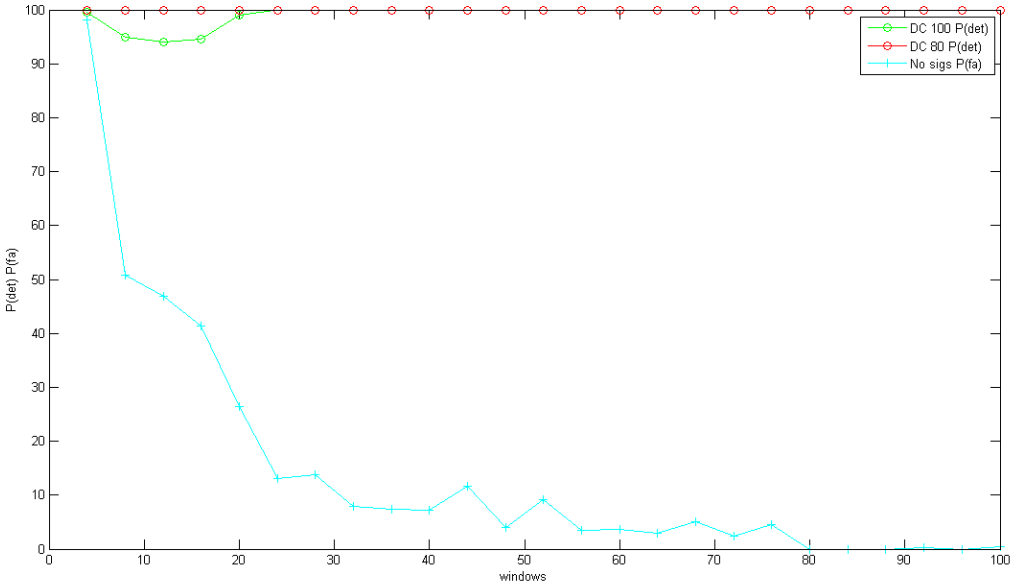

Figure 4-13 Reliability: 8 subcarrier sig, threshold 0.3, receive power -85dBm

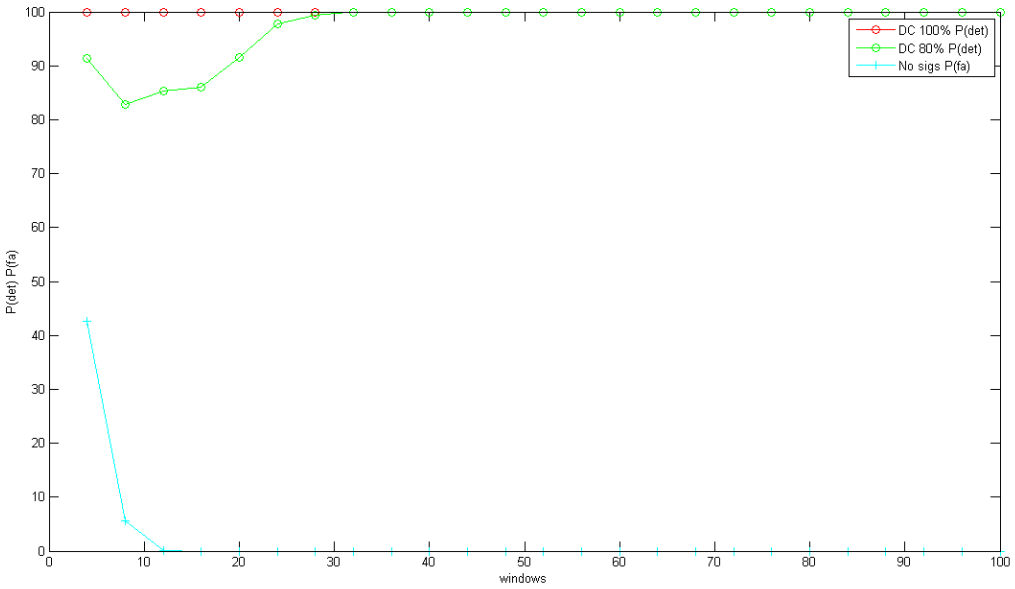

Figure 4-14 Reliability: 8 subcarrier sig, threshold 0.4, receive power -85dBm

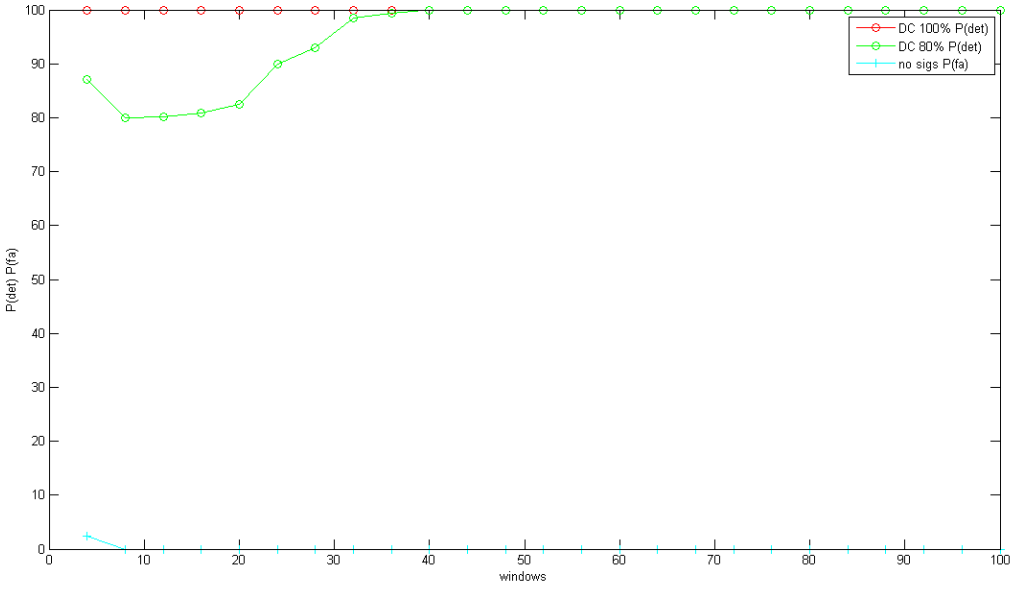

Figure 4-15 Reliability: 8 subcarrier sig, threshold 0.5, receive power -85dBm

4.3.3- **Graphs of reliability experiments with 4 subcarrier signatures, -75dBm**

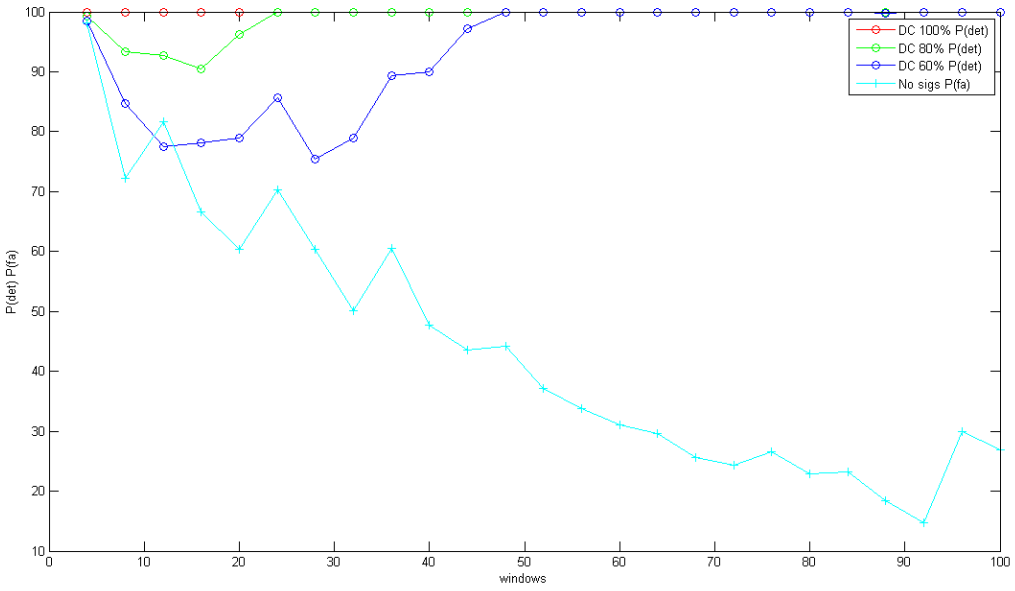

Figure 4-16 Reliability: 4 subcarrier sig, threshold 0.3, receive power -75dBm

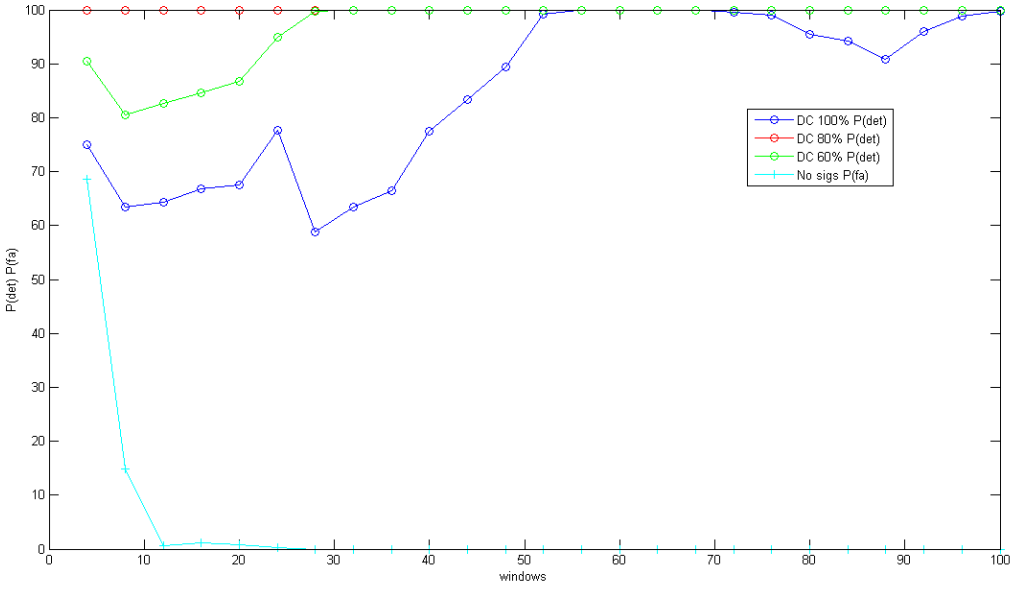

Figure 4-17 Reliability: 4 subcarrier sig, threshold 0.4, receive power -75dBm

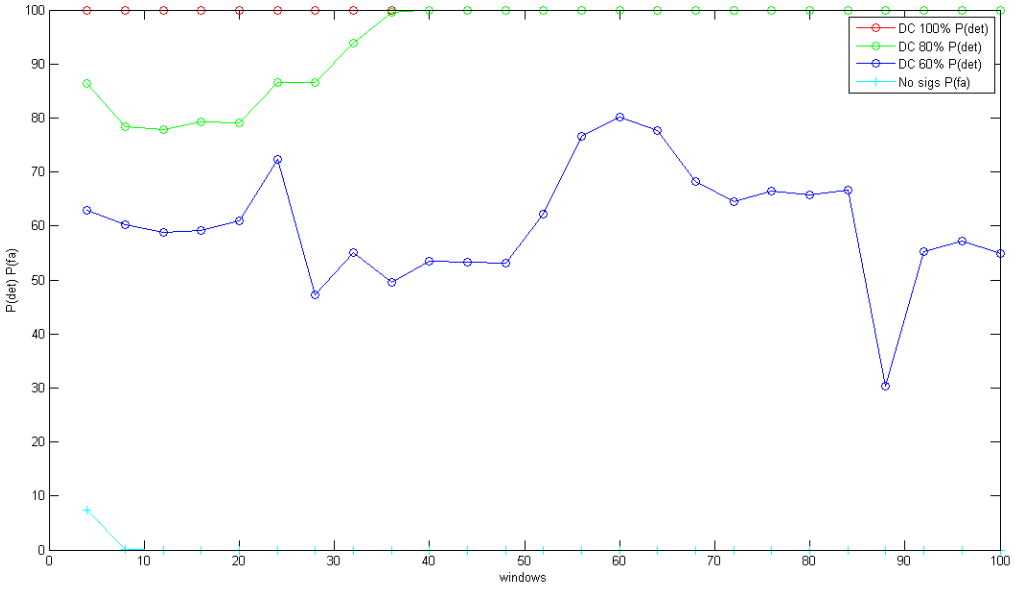

Figure 4-18 Reliability: 4 subcarrier sig, threshold 0.5, receive power -75dBm

4.3.4- **Graphs of reliability experiments with 4 subcarrier signatures, -85dBm**

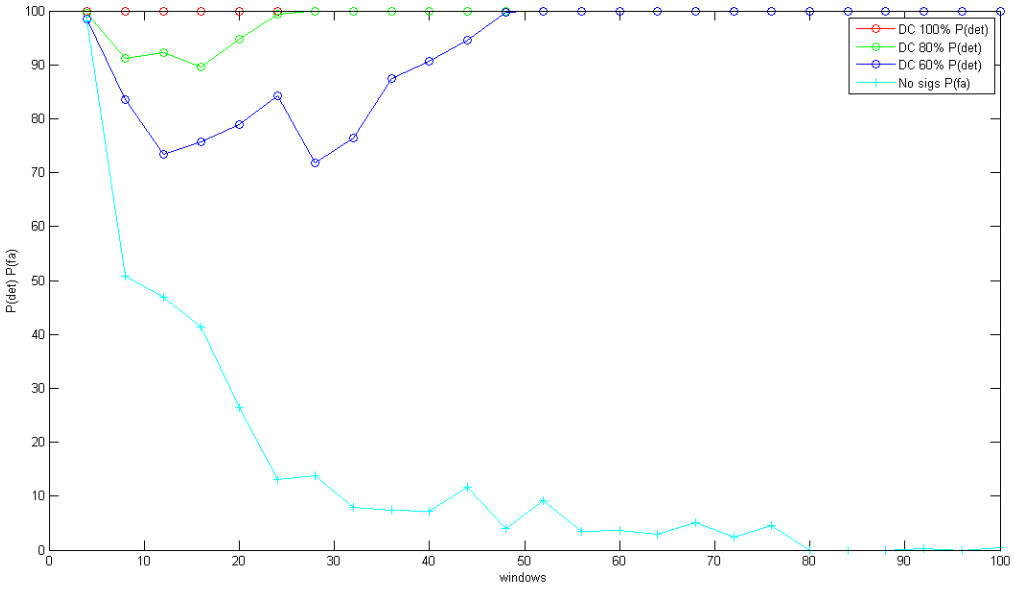

Figure 4-19 Reliability: 4 subcarrier sig, threshold 0.3, receive power -85dBm

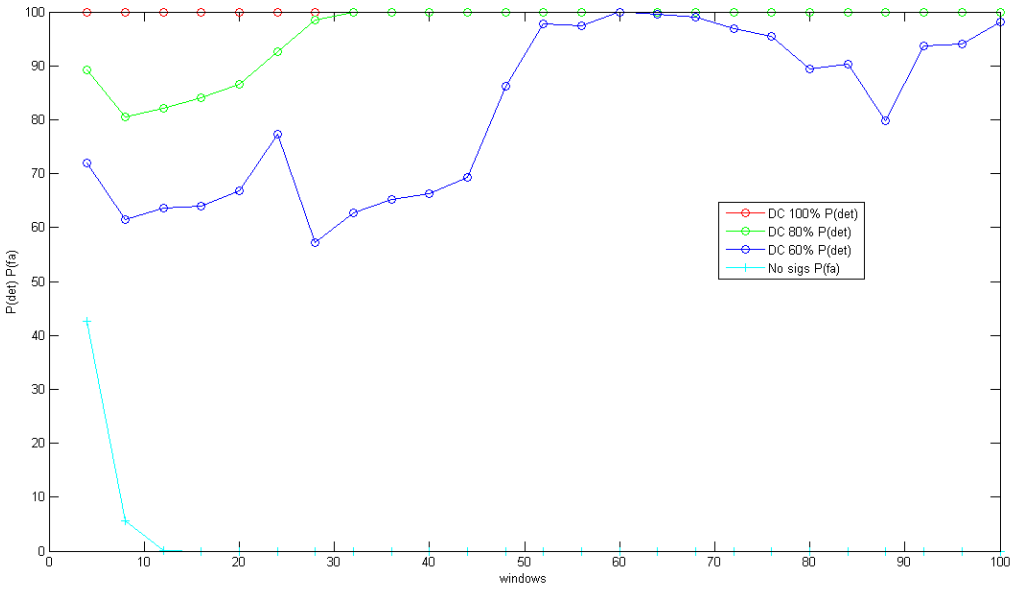

Figure 4-20 Reliability: 4 subcarrier sig, threshold 0.4, receive power -85dBm

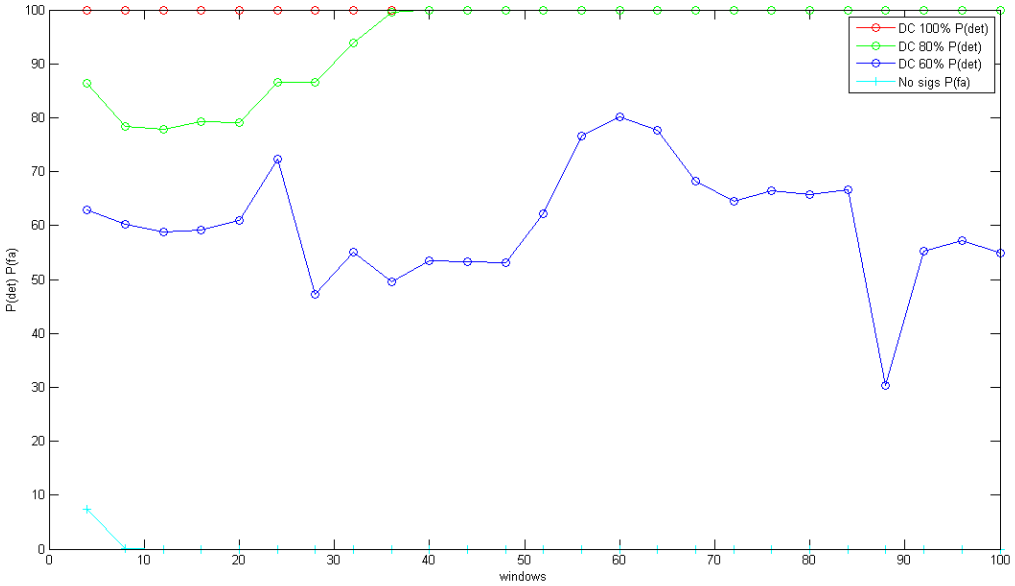

Figure 4-21 Reliability: 4 subcarrier sig, threshold 0.5, receive power -85dBm

4.3.5- **Discussion of TTR performance results**

It is immediately apparent, looking at Figure 4-10 Figure 4-13, Figure 4-16 and Figure 4-19, where the threshold is 0.3, that the P(fa) = 0 is not achieved when the received signal strength is at -75dBm within the allowed range of observation windows, which top out at 100. In the case of the weaker received signal strength, it takes a large observation time, 80 windows, for a P(fa) of 0 to be achieved. This is the case for signatures of both 8 and 4 mapped subcarriers. This immediately rules out the use of the lower threshold setting under these scenarios.

It can be seen that choosing a higher threshold is necessary to account for a noisier environment; the P(fa) drops off significantly as it is increased from 0.3 to 0.5.

For the scenarios where the threshold was set at 0.4, as shown in Figure 4-11, Figure 4-14, Figure 4-17 and Figure 4-20,it can be observed a P(fa) of 0 is achieved at 28 windows when the received power is -75dBm, falling to 12 windows at the lower receive power. This is a considerable improvement on the false alarm rate for the lower 0.3 threshold.

Looking at Figure 4-11 and Figure 4-17 it can be seen that the P(det) for both an 8 subcarrier signature and 4 subcarrier signature received at -75dBm, at both DC =100% and 80%, is 100% at a window size of 28, where the P(fa) is 0. This indicates that there is no benefit to using the larger signature in these conditions. Returning to the results in the previous section it can also be observed that there is no TTR advantage to using the larger signature in this scenario either.

As noted, where the weaker received signal was used, as shown in Figure 4-14 and Figure 4-20, for a threshold of 0.4, a P(fa) of 0 is achieved for a window size of just 12. While, the P(det) is 100% for a non-bursty signal at this point, for both the 4 and 8 subcarrier signals, when the duty cycle drops to 80% it is necessary to have a larger window or 32. However, looking at the results from the previous section it can be observed that the TTR is only marginally increased; an 8 subcarrier signature could be detected within 1.08s at 12 windows whereas a 4 subcarrier signature would be detected within 1.28s at 32 windows (see Figure 4-6 and Figure 4-8).

Turning the scenarios where the threshold is set at 0.5 it is immediately apparent that the signals with the least embedding of the signature, i.e. those at DC = 60% are completely unreliable. This is a result of the of the decision threshold being so high that the detector cannot give a positive indication owing to

the fact that signatures are not consistently present. For the scenario where the signal contains an embedded signature at least 80% of the time then the P(det) deteriorates only slightly compared to the scenario where the threshold is 0.4. It now takes the detector 40 windows to achieve a 100% detection probability, whereas it was 32 windows for the case of a 0.4 threshold. However, the higher decision threshold of 0.5 does result in a lower wait to achieve a P(fa) of 0%; this is now achieved at 8 windows, see Figure 4-12, Figure 4-15, Figure 4-18, and Figure 4-21.

Overall, it can be seen that the P(det) figures for a signal where the embedded signature is only present 60% of the time do not yield results which display any predictability. Again, owing to the effects of the correlation of the window size with the burstiness of the signal, as explained in the previous section, the detector is unable to account for the signals burstiness in its process. This suggests that signals displaying this characteristic are not suitable for Rendezvous. As such, it becomes incumbent on the master device transmitting the signal to ensure that the embedded signature is transmitted where the duty cycle approaches, or exceeds, 80%.

Furthermore, where the signal contains a constantly embedded signature the experimental results show that the detector is capable of achieving the lowest TTR figures possible (as described in the previous section) for a P(fa) of 0% and a P(det) of 100%. For example, referring to Figure 4-2 and Figure 4-12, it can be seen that a 8 subcarrier signal received at -75dBm, with observation window set at 12, can be detected in 1.053s with a P(fa) of 0% and a P(det) of 100%.

4.4- **Summary**

The Rendezvous detector has been shown to exhibit robust properties in a real setting with radios operating in TVWS frequencies. The experiments were conducted to evaluate the performance of the Rendezvous detector with regard to its key objectives; the speed at which Rendezvous can be achieved (measured by TTR), and the reliability and accuracy with which that Rendezvous occurs.

From the perspective of TTR it was shown that in order to guarantee a linear, and predictable, detector performance, the window size should be chosen such that it lies in an area that, when combined with the burstiness of the signal, gives a certain guarantee of performance. For signals with a constant signature presence, the optimum observation window size is between 8 and 20 windows; this is true for signatures of all sizes. For signals with 80% signature presence, the optimum range for window size is 15 to 25. The effect of increasingly bursty signals on the detector is exacerbated in the case of the a signal with a signature presence of about 60%; it can be seen that a large observation window is required to attain predictable behavior from the detector.

From the perspective of reliability and accuracy it was shown that the detector operates well within the window ranges indicated by the TTR experiments. More specifically, the detector for can achieve the lowest TTR measurements obtained in the laboratory experiments for settings which also ensure 100% reliability and accuracy.

5- Conclusions

Our inspection of the WBX board indicates that there are a number of spurious emissions located at a number of different frequencies which need to be filtered for transmission in the TV Bands. Given that the WBX was being targeted to the frequency range 694MHz to 718MHz we were able to distinguish between in-band and out of band spurious emissions. The in-band emissions were contained within our band of operation and so were not of concern as we were able to accommodate both the wanted signal and these unwanted emissions within the licenced bandwidth. However, the out-of-band emmissions occurred at a number of frequencies across the range of the WBX board and in particular in the 2GHz UMTS band. A custom-made bandpass filter which addressed these out-of-band emissions was made to address this problem.

In order to achieve an output power approaching the limit of our licensed permission, of 100mW, a COTS amplifier, suited to the frequency range in use, was acquired. This allowed us to operate the WBX on-board amplifier in such a way that it did not distort the transmitted signal. Instead the, approximately 18 dB was achieved using the power amplifier. Should the licensed range of experimental operation change, a new bandpass filter can be made.

The Spectrum Shaping component of the TVWS Transceiver was evaluated to see how it performed when constrained by a Block Edge mask. It was shown that the spectrum shaping mechanisms work efficiently under certain limitations caused by USRP frontend (intermodulations, only some sampling frequencies allowed), and the limitations of the host PC (computational complexity).

The link capacity was shown to be only slightly dependent on the spectrum shaping algorithms (throughput decrease because of CCs and windowing introduction, SNR loss negligible).

It was shown that the time domain synchronization can be disturbed by cancellation carriers and interference from primary systems; thus an efficient synchronization strategy for situations where the TVWS operates under strong interference from primary devices is required. For now we need 20 dB SIR for correct transmission in the presence of PMSE device.

Spectrum shaping was shown to give an improvement not only on PSD plot, but also for end user QoS experience. With the same spectrum occupation (narrow notch) we were able to increase secondary user power by e.g. 8 dB providing the same sound quality to PMSE device user.

The Rendezvous detector has been shown to exhibit robust properties in a real setting with radios operating in TVWS frequencies. The experiments were conducted to evaluate the performance of the Rendezvous detector with regard to its key objectives; the speed at which Rendezvous can be achieved (measured by TTR), and the reliability and accuracy with which that Rendezvous occurs.

From the perspective of TTR it was shown that in order to guarantee a linear, and predictable, detector performance, the window size should be chosen such that it lies in an area that, when combined with the burstiness of the signal, gives a certain guarantee of performance. For signals with a constant signature presence, the optimum observation window size is between 8 and 20 windows; this is true for signatures of all sizes. For signals with 80% signature presence, the optimum range for window size is 15 to 25. The effect of increasingly bursty signals on the detector is exacerbated in the case of the a signal with a signature presence of about 60%; it can be seen that a large observation window is required to attain predictable behavior from the detector.

From the perspective of reliability and accuracy it was shown that the detector operates well within the window ranges indicated by the TTR experiments. More specifically, the detector for can achieve the lowest TTR measurements obtained in the laboratory experiments for settings which also ensure 100% reliability and accuracy.

6- References

[1] COGEU FP7 ICT-2009.1.1, “D5.2 Algorithms for cognitive spectrum shaping and advanced rendezvous”.

[2] COGEU FP7 ICT-2009.1.1, “D5.3 COGEU TVWS transceiver integration”.

[3] COGEU FP7 ICT-2009.1.1, “D5.1 COGEU transceiver platform specification”.

[4] ETSI TS 136 101 V10.3.0 (2011-06) LTE; Evolved Universal Terrestrial Radio Access (E-UTRA); User Equipment (UE) radio transmission and reception (3GPP TS 36.101 version 10.3.0 Release 10)

[5] COGEU FP7 ICT-2009.1.1, “D3.1 Use-cases Analysis and TVWS Systems Requirements”.

[6] Federal Communications Commission “Unlicensed Operation in the TV Broadcast Bands; Final Rule”, 6th December 2010

[7] T. M. Schmidl, D. C. Cox, "Robust frequency and timing synchronization for OFDM," IEEE Transactions on Communications, vol.45, no.12, pp.1613-1621, Dec 1997

[8] ETSI TR 102 546 V1.1.1 (2007-02) Electromagnetic compatibility and Radio spectrum Matters (ERM); Technical characteristics for Professional Wireless Microphone Systems (PWMS); System Reference Document

List of Tables

List of Figures

List of Abbreviations

3GPP	3rd Generation Partnership Project
ACLR	Adjacent Channel Leakage Ratio
ATSC	Advanced Television Systems Committee
CC	Cancellation Carrier
COTS	Commercial Off The Shelf
CR	Cognitive Radio
DVB-H	Digital Video Broadcasting – Handheld
DVB-T	Digital Video Broadcasting - Terrestrial
FCC	Federal Communications Commission
IEEE	The Institute of Electrical and Electronics Engineers
ISM	Industrial Scientific and Medical (band)
LTE	Long Term Evolution
MIMO	Multiple-Input Multiple-Output
NC-OFDM	Non-contiguous OFDM
OFDM	Orthogonal Frequency Division Multiplexing
OOB	Out of Band (emission)
PAPR	Peak to Average Power Ratio
PMSE	Programme Making and Special Events
PWMS	Professional Wireless Microphone Systems
QoS	Quality of Service
RF	Radio Frequency
SDR	Software Defined Radio
SNR	Signal to Noise Ratio
TTR	Time To Rendezvous
TV	Television
TVWS	TV White Spaces
UHF	Ultra High Frequency
UMTS	Universal Mobile Telecommunications System
USRP	Universal Software Radio Peripheral
WP	Work Package